



## PtdIns4P exchange at endoplasmic reticulum-autolysosome contacts is essential for autophagy and neuronal homeostasis

Hao Liu<sup>a,b\*</sup>, Wenxia Shao<sup>a,b\*</sup>, Wei Liu<sup>a,b</sup>, Weina Shang<sup>a</sup>, Jun-Ping Liu<sup>c</sup>, Liqian Wang<sup>b</sup>, and Chao Tong<sup>a,b,c,d</sup>

<sup>a</sup>MOE Key Laboratory for Biosystems Homeostasis & Protection and Innovation Center for Cell Signaling Network, Life Sciences Institute, Zhejiang University, Hangzhou, Zhejiang, China; <sup>b</sup>Department of Gastroenterology of the Second Affiliated Hospital, School of Medicine, Zhejiang University, Hangzhou, Zhejiang, China; <sup>c</sup>Institute of Aging Research, Hangzhou Normal University, Hangzhou, Zhejiang, China; <sup>d</sup>Institute of Neurological and Psychiatric Disorders, Shenzhen Bay Laboratory, Shenzhen, Guangdong, China

### ABSTRACT

Inter-organelle contacts enable crosstalk among organelles, facilitating the exchange of materials and coordination of cellular events. In this study, we demonstrated that, upon starvation, autolysosomes recruit Pi4KII $\alpha$  (Phosphatidylinositol 4-kinase II  $\alpha$ ) to generate phosphatidylinositol-4-phosphate (PtdIns4P) on their surface and establish endoplasmic reticulum (ER)-autolysosome contacts through PtdIns4P binding proteins Osbp (Oxysterol binding protein) and cert (ceramide transfer protein). We found that the Sac1 (Sac1 phosphatase), Osbp, and cert proteins are required for the reduction of PtdIns4P on autolysosomes. Loss of any of these proteins leads to defective macroautophagy/autophagy and neurodegeneration. Osbp, cert, and Sac1 are required for ER-Golgi contacts in fed cells. Our data establishes a new mode of organelle contact formation – the ER-Golgi contact machinery can be reused by ER-autolysosome contacts by re-locating PtdIns4P from the Golgi apparatus to autolysosomes when faced with starvation.

**Abbreviations:** Atg1: Autophagy-related 1; Atg8: Autophagy-related 8; Atg9: Autophagy-related 9; Atg12: Autophagy-related 12; cert: ceramide transfer protein; Cp1/CathL: cysteine proteinase-1; CTL: control; ER: endoplasmic reticulum; ERMCS: ER-mitochondria contact site; fwd: four wheel drive; GM130: Golgi matrix protein 130 kD; Osbp: Oxysterol binding protein; PG: phagophore; PtdIns4K: phosphatidylinositol 4-kinase; Pi4KII $\alpha$ : Phosphatidylinositol 4-kinase II  $\alpha$ ; Pi4KIII $\alpha$ : Phosphatidylinositol 4-kinase III  $\alpha$ ; PtdIns4P: phosphatidylinositol-4-phosphate; PR: photoreceptor cell; RT: room temperature; Sac1: Sac1 phosphatase; Stv: starvation; Syx17: Syntaxin 17; TEM: transmission electron microscopy; VAP: VAMP-associated protein.

### ARTICLE HISTORY

Received 3 July 2022;  
Revised 12 May 2023;  
Accepted 2 June 2023

### KEYWORDS



*Drosophila*; endoplasmic reticulum-autolysosome contacts; Golgi apparatus; PtdIns4P; autophagy

## Introduction

The cytosol of eukaryotic cells contains different organelles that perform various cellular functions. Different organelles form close contacts (10–30 nm) to exchange materials, coordinate cellular events, and respond to various stimuli [1,2]. The ER is the center of protein synthesis, lipid synthesis, and calcium storage in eukaryotic cells. ER is a large tubular network of membranes that forms contacts with the plasma membrane and various other organelles, such as mitochondria, Golgi apparatus, endosomes, and lysosomes in the cytosol [3–5].


The ER usually forms contacts with other organelles through interactions between ER-anchored proteins and proteins located on the membrane of other organelles [6]. VAPs (VAMP-associated proteins) are key ER-resident proteins that mediate multiple interactions between the ER and other organelles [7]. The major sperm protein domain of VAPs interacts with proteins containing a FFAT (i.e., diphenylalanine in an acidic tract) motif [8]. There are many FFAT motif

containing proteins, such as the mitochondrial proteins RMDN3/PTPIP51 (regulator of microtubule dynamics 3) and Miga (Mitoguardin) [5,9,10], endosome proteins STARD3 (StAR related lipid transfer domain containing 3) and STARD3NL (STARD3 N-terminal like) [11], and Golgi-associated proteins OSBP, CERT1, PLEKHA8/FAPP2 (pleckstrin homology domain containing A8), and PITPNM1/NIR2 (phosphatidylinositol transfer protein membrane associated 1) [12], whose interactions with VAPs establish contacts between the ER and various other organelles. Contacts between the ER and other organelles regulate many pivotal cellular processes, including macroautophagy (referred to as autophagy hereafter) [13]. Autophagy is a self-digestion process that is critical for cellular homeostasis [14]. Starvation and other stresses lead to the inhibition of the TOR pathway, followed by the activation of Atg1 and phosphatidylinositol 3-kinase (PtdIns3K) complexes to initiate the autophagy process. By orchestrating complexes, such as Atg12–Atg5–Atg16 and Atg2–Atg9–Atg18, and phosphatidylethanolamine (PE)

**CONTACT** Chao Tong  [ctong@zju.edu.cn](mailto:ctong@zju.edu.cn)  MOE Key Laboratory for Biosystems Homeostasis & Protection and Innovation Center for Cell Signaling Network, Life Sciences Institute, Zhejiang University, 866 Yuhangtang Rd, Hangzhou 310058, China

\*These authors contributed equally to this work.

This article has been corrected with minor changes. These changes do not impact the academic content of the article.

 Supplemental data for this article can be accessed online at <https://doi.org/10.1080/15548627.2023.2222556>.

© 2023 Informa UK Limited, trading as Taylor & Francis Group

modification of Atg8, the phagophore (PG) engulfs substrates to form Atg8-labeled autophagosomes [15]. The soluble N-ethylmaleimide – sensitive factor attachment protein receptor (SNARE) complex and other tethering complexes further facilitate fusion between autophagosomes and late endosomes/lysosomes to form amphisomes and autolysosomes. The substrates are then digested in autolysosomes to release nutrients and promote lysosomal regeneration [16]. Many sophisticated mechanisms regulate the autophagy process. Autophagy is initiated at the ER-mitochondria contact sites (ERMCSs). In cultured mammalian cells, the ER-resident SNARE protein STX17 (syntaxin 17) is translocated to ERMCSs upon starvation. It recruits ATG14 (autophagy related 14) to contacts and triggers autophagosome formation [17]. Increased ERMCS formation by overexpressing tether proteins, such as VAPB and RMDN3/PTPIP51, inhibits autophagy; conversely, the weakening of contacts stimulates autophagosome formation [18]. Mitochondrial respiration supports autophagy through the regulation of ERMCS formation [19]. In addition to ERMCSs, PG dynamically interact with the ER during autophagosome formation in mammalian cells. VAPs directly interact with RB1CC1/FIP200 (RB1 inducible coiled-coil 1), ULK1 (unc-51 like autophagy activating kinase 1), and WIPI2 (WD repeat domain, phosphoinositide interacting 2) to promote ER-PG contact formation. Depletion of the ER-localized autophagy protein VMP1/EPG-3 (vacuole membrane protein 1) elevates the interaction of VAPs with these autophagy proteins and increases ER-PG contact formation [20,21]. These studies indicate that early autophagy-related structures are closely associated with the ER, and that these contacts are critical for the initiation of autophagy; however, it is unclear whether there is contact between the ER and late-stage autophagic structures, such as autolysosomes. If there are such contacts, it is unknown what mediates them and how they function during the autophagy process.

In this study, we demonstrated that the loss of phosphatidylinositol 4-phosphate phosphatase *Sac1* led to neurodegeneration and autophagy defects in *Drosophila*. In animals with reduced levels of *Sac1*, autophagy initiation was upregulated, but the autophagy flux was slightly reduced due to the reduction in autolysosomal acidification. There was no autophagosome-lysosome fusion defect in *Sac1* mutants, which is different from what has been reported in yeast [22]. We found that the reduction of *Sac1* increased the level of PtdIns4P on autolysosomes. We also observed increased contacts between the ER and autolysosomes.

*Sac1* is a critical player in ER-Golgi contact formation [23]. Lipid transfer proteins, such as OSBP and CERT1, bind to PtdIns4P-enriched Golgi compartments and transfer cholesterol and/or ceramide from the ER to the Golgi apparatus. OSBP also transfer PtdIns4P to the ER. ER-localized SACM1L hydrolyzes PtdIns4P to maintain the concentration gradient of PtdIns4P between the Golgi apparatus and the ER, thereby sustaining the lipid transfer processes [23].

PtdIns4P is mainly localized on the plasma membrane and Golgi apparatus in fed tissues and is transferred to the surface of autolysosomes upon starvation. PtdIns4P is synthesized by phosphatidylinositol 4-kinases (PtdIns4Ks) [24–26].

Mammals have two type II and two type III PtdIns4Ks (PI4K2A, PI4K2B, PI4KA, PI4KB), whereas flies have a single type II PtdIns4K (Pi4KII $\alpha$ ) and two type III enzymes (fwd [four wheel drive] and Pi4KIII $\alpha$  [Phosphatidylinositol 4-kinase III  $\alpha$ ]). In yeast, two major yeast PtdIns4Ks, Pik1 and Stt4, are both required for autophagy [27]. In mammals, PI4K2A is required for the fusion between autophagosomes and lysosomes. PI4K2A resides in the trans-Golgi under fed conditions but relocates to autophagosomes through interaction with GABARAPs during autophagy [28]. However, the role of PtdIns4P in this scenario is not clear. It is also unclear whether downstream effectors of PtdIns4P participate in the late stages of autophagy.

In this study, we determined that all three PtdIns4Ks were required for autophagy, but Pi4KII $\alpha$  mainly contributed to autophagy-induced PtdIns4P accumulation on autolysosomes. We also found that autolysosomal-enriched PtdIns4P recruits Osbp and cert, but not other PtdIns4P-binding proteins, such as Arfp (Arfaptin) or sau (sauron) [29,30]. The loss of *Osbp* or *cert* led to autophagy defects similar to but less severe than the loss of *Sac1*. We propose a model wherein, upon autophagy, the translocation of Pi4KII $\alpha$  triggers the production of PtdIns4P to the autolysosomes, which recruits downstream effectors, such as Osbp and cert, to form ER-autolysosome contacts. Lipid transfer at contacts is critical for proper autophagy and neuronal homeostasis.

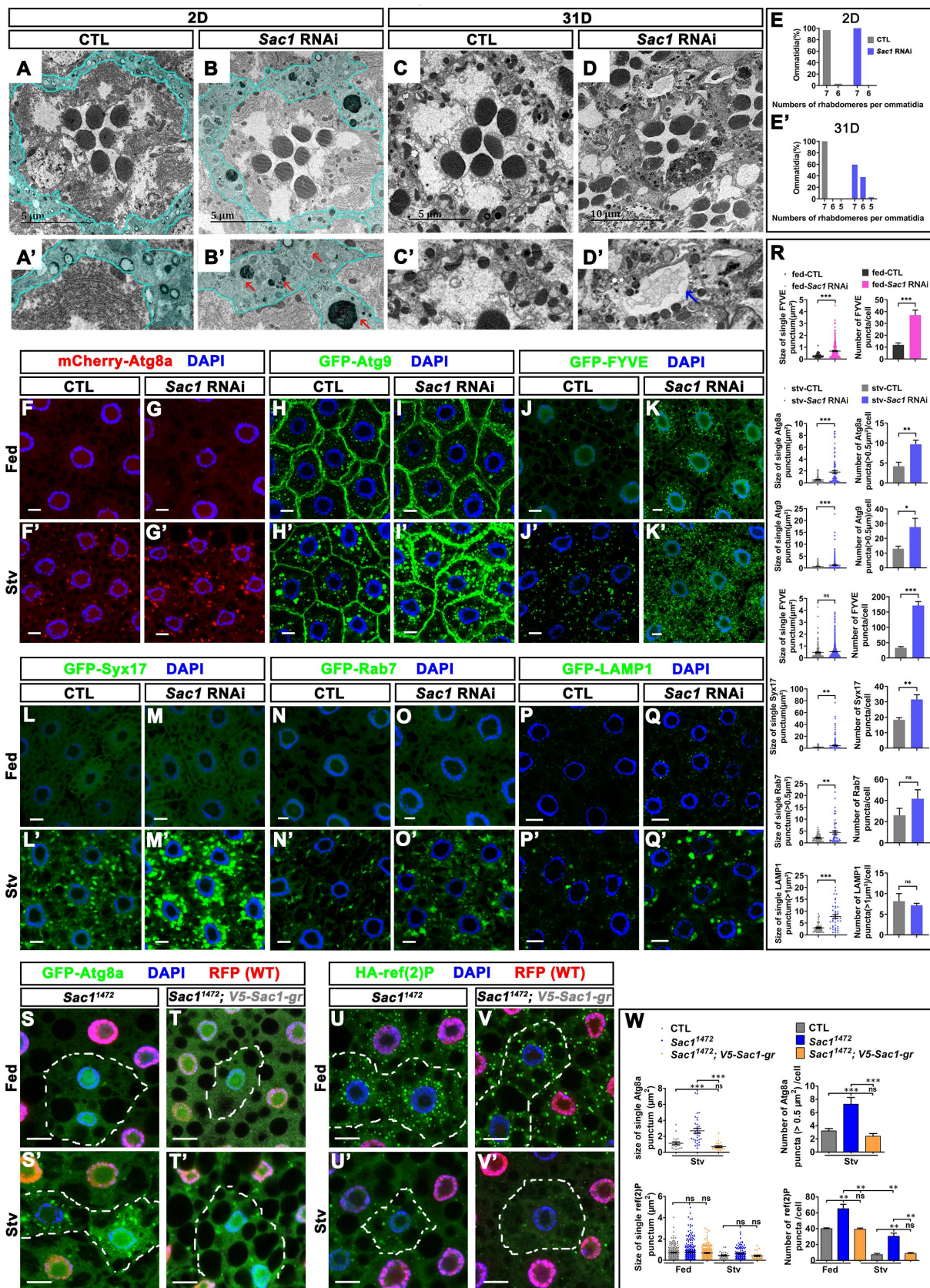
## Results

### *Sac1* was required for neuronal homeostasis and proper autophagy

To examine the function of PtdIns4P phosphatase *Sac1* in fly eyes, we used GMR-Gal4 driving UAS-shRNA expression in fly eyes and examined retinal morphology in young (i.e., 2-day-old) and aged (i.e., 31-day-old) flies by transmission electron microscopy (TEM) (Figure 1A–E', Figure S1A – K). In young control flies, seven photoreceptor cells (PRs) were wrapped with a thin layer of glial cells (pigment cells) (Figure 1A, A'). In aged control flies, the glial cell layer became too thin to be distinguished and the seven PRs were intact (Figure 1C, C'). In 2-day old flies, the reduction in *Sac1* had no obvious effects on the number and morphology of PRs; however, the glial cell layer was swollen and double-membraned autophagosomes and electron-dense autolysosomes accumulated (Figure 1B, B', Figure S1C, C', and J). In aged flies with *Sac1* knockdown, some rhabdomeres of PRs were degenerated, and there were some empty spaces between ommatidia, a sign of the loss of glial cells (Figure 1D, D', Figure S1D, D', I, and K). We next evaluated whether the degeneration caused by *Sac1* RNAi was due to the reduction in *Sac1*. We knocked down *Sac1* expression and overexpressed hemagglutinin (HA)-tagged *Sac1* in the developing eyes. As a control, we overexpressed red fluorescent protein (RFP) in eyes with *Sac1* knockdown. Overexpression of *Sac1*, but not that of RFP, rescued eye degeneration in *Sac1* RNAi animals (Figure S1A – F', I – K).

The degeneration of PRs and glial cells was intriguing, and the accumulation of autophagosomes/autolysosomes in young





fly eyes suggested that the loss of *Sac1* might lead to an abnormal autophagy. We then examined whether *Sac1* was required for autophagy in the fly fat body, which is a model tissue used to study the autophagy process. We used Cg-Gal4, a fat body expressing Gal4, to drive *Sac1* siRNA expression, together with various autophagy markers (Figure 1F–R). Knockdown of *Sac1* in the fat bodies was confirmed by real-time PCR (Figure S2A). Under fed conditions, most autophagy markers did not change upon *Sac1* RNAi treatment (Figure 1F–R), except for the PtdIns3P reporter GFP-FYVE, whose levels slightly increased (Figure 1J, K, and R). Upon starvation, the reduction of *Sac1* led to an increase in all the autophagy markers assessed, including autophagosome markers mCherry-Atg8a (Figure 1F', G', and R), GFP-Atg9 (Figure 1H', I', and R), GFP-FYVE (Figure 1J', K', and R), GFP-Syx17 (Syntaxin 17) (Figure 1L', M', and R), late endosome marker GFP-Rab7 (Figure 1N', O', and R), and lysosome marker GFP-LAMP1 (Figure 1P', Q', and R). This suggested that autophagy was perturbed upon loss of *Sac1*. The patterns of endogenous proteins, such as autophagy marker Atg8a and lysosome marker Cp1/CathL (Cysteine protease-1), were also examined in control and *Sac1* RNAi tissues under both fed and starvation conditions. Both proteins form puncta during starvation (Figure S2B – G). The size and number of puncta increased in *Sac1* RNAi tissues upon starvation (Figure S2B', C', D, E', F', and G). Atg8a is a ubiquitin-like protein that can be processed and modified by phospholipids to form a short form (Atg8a-II) under starvation conditions. Atg8a-II labels autophagosomes and is digested in autolysosomes. We measured the ratio of Atg8a-II to Atg8a-I (unprocessed long form of Atg8a) using western blotting. This ratio increased in the *Sac1* RNAi tissues under starvation conditions (Figure S3A, A'), suggesting that the reduction in *Sac1* led to abnormal autophagy. To confirm that the abnormal autophagy phenotypes were indeed due to the loss of *Sac1*, we examined the patterns of GFP-Atg8a and HA-ref(2)P/SQSTM1/p62, an autophagy substrate, in *Sac1* mutant clones (Figure 1S–W). Like what we observed in *Sac1* RNAi tissues, GFP-Atg8a and HA-ref(2)P accumulated in *Sac1* (*Sac1*<sup>1472</sup>) mutant clones and could be rescued by introducing a genomic fragment containing only *Sac1* gene (Figure 1S–W) [31]. These data suggested that *Sac1* was required for autophagy and neuronal homeostasis in the flies.

### **The loss of *Sac1* promoted autophagosome formation, but failed to fully digest the substrates**

To fully understand the defects in autophagy upon the reduction of *Sac1*, we measured autophagy flux in fat body tissues. We expressed GFP-RFP-Atg8a in fat bodies and examined its expression pattern in fed and starved animals with or without

*Sac1* knockdown (Figure 2A–B' and G). Under fed conditions, GFP-RFP-Atg8a was diffused in both control and *Sac1* RNAi animals (Figure 2A and B). Upon starvation, red puncta were observed in the control animals because of quenching of GFP in the acidic autolysosomes (Figure 2A'). However, in *Sac1* RNAi animals, the puncta were all yellow, and the number of puncta increased, suggesting a reduction in autophagy flux (Figure 2B' and G). We then examined the autophagy substrate ref(2)P. Compared with the control (Figure 2C and C'), puncta sizes were slightly increased in *Sac1* RNAi tissues under both fed (Figure 2D) and starvation conditions (Figure 2D', H, and H'), suggesting that autophagy flux was reduced in *Sac1* RNAi tissues. However, in *Sac1* RNAi animals, both the size and number of HA-ref(2)P under starvation conditions (Figure 2D') were lower than those under fed conditions (Figure 2D, H, and H'). These data suggested that autophagy flux was hindered, but not completely blocked, by the reduction of *Sac1*. The GFP signals of GFP-RFP-Atg8a failed to be quenched in *Sac1* RNAi tissues, suggesting that either Atg8a labeled autophagosomes failed to fuse with lysosomes or the pH of the autolysosomes was not low enough to quench GFP. We then examined the pH of the autolysosomes using the yellow/blue LysoSensor and found that the pH of the puncta structures in *Sac1* RNAi tissues was higher than that in the control tissues (Figure 2E–F' and I). We further explored whether autophagosomes fuse with lysosomes in *Sac1* RNAi tissues. Syx17 labels fully formed autophagosomes and Cp1 labels lysosomes [32]. In fed control animals, Syx17 was largely diffused, and Cp1 signals were weak (Figure 2J). Upon starvation, both Syx17 and Cp1 formed large puncta, many of which were colocalized in control animals (Figure 2J', J''). In *Sac1* RNAi fat bodies, both Syx17 and Cp1 signals increased and the large puncta of Syx17 and Cp1 were colocalized under starvation conditions (Figure 2K', K''). We also labeled autophagosomes with mCherry-Atg8a and lysosomes with HRP-LAMP1 (Figure 2L–M''). Both Atg8a and LAMP1 puncta increased in starved *Sac1* RNAi tissues, and the two markers colocalized with each other (Figure 2M', M''), suggesting that autophagosomes fused with lysosomes. We also examined whether *Sac1* mutant cells had an autophagosome-lysosomal fusion defect. We labeled autophagosome with GFP-Atg8a and stained the fat bodies carrying *Sac1*<sup>1472</sup> mutant clones with antibody recognizing lysosome marker Cp1. The accumulated GFP-Atg8a colocalized with Cp1 in the cells, suggesting that the autophagosomes and lysosomes were fused in the mutant clones (Figure S3E – H).

We then examined the ultrastructures of the early third-instar larval fat bodies. Under fed conditions, electron-dense autolysosomes were not observed in control fat bodies (Figure 2N, R) but could occasionally be found in *Sac1* RNAi tissues (Figure 2O, R). Upon starvation, autophagosomes and

GFP-FYVE under both fed and starvation conditions. The puncta of mCherry-Atg8a, GFP-Atg9, GFP-Syx17, GFP-Rab7, and GFP-LAMP1 were increased in the *Sac1* RNAi tissues during starvation. DAPI marked the nuclei. Scale bar: 10  $\mu$ m. (S – V) Under the fed and starvation conditions, the patterns of GFP-Atg8a (S – T) or HA-ref(2)P (U – V) were examined in the mosaic fat body tissues containing *Sac1* mutant (*Sac1*<sup>1472</sup>) clones (marked by loss of RFP and outlined by dash lines) with or without a genomic DNA fragment containing *Sac1* gene with a cDNA encoding V5 tag inserted just after the start codon (V5-*Sac1*-gr). (W) was the quantification for the experiments in (S'–V'). The size and number of GFP-Atg8a and HA-ref(2)P puncta in the cells with indicated genotypes were quantified. The RFP-positive cells in the mosaic tissues served as CTL. GFP-Atg8a and HA-ref(2)P were accumulated in the *Sac1* mutant clones and the genomic rescue constructs rescued the phenotypes.  $n = 4$ , ns: not significant, \*\*:  $p < 0.01$ , \*\*\*:  $p < 0.001$ . DAPI marked the nuclei. Scale bar: 10  $\mu$ m.



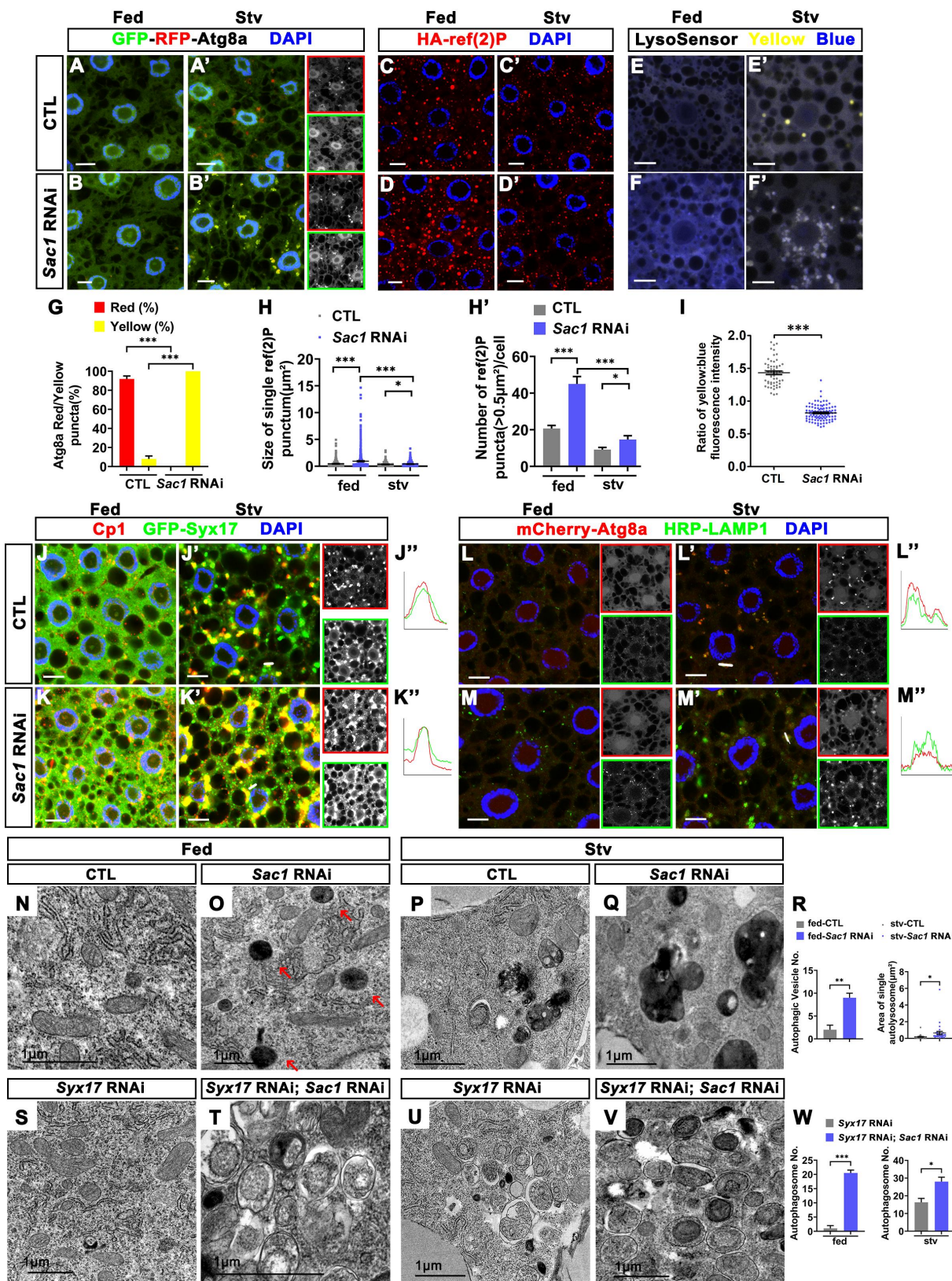


**Figure 2.** Autophagy was induced but partially blocked at late stage upon the reduction of *Sac1*. The expression of *Sac1* was reduced in fly fat bodies by RNAi. The autophagy markers were examined in fat bodies of the early third-instar larvae under fed and starvation conditions. (A – B') GFP-RFP-Atg8a formed red puncta upon starvation in the control tissues (A'). GFP-RFP-Atg8a puncta were yellow in the *Sac1* RNAi tissues (B'). The red or green channels were split and shown as gray scale images next to the merged images. The red or green channels were outlined by red or green, respectively. The quantification of the percentage of red and yellow puncta was shown in (G).  $n = 6$ , \*\*\*,  $p < 0.001$ . (C – D') There were more HA-ref(2)P puncta accumulated in the *Sac1* RNAi fat bodies than those in CTL fat bodies under both fed and starvation conditions. HA-ref(2)P puncta were reduced upon starvation in both CTL and *Sac1* RNAi tissues. (H and H') were quantifications of the sizes and numbers of HA-ref(2)P puncta in CTL and *Sac1* RNAi tissues under fed and starvation conditions.  $n = 6$ , \*,  $p < 0.05$ ; \*\*\*,  $p < 0.001$ . (E – F') LysoSensor yellow/blue staining of the CTL and *Sac1* RNAi fat bodies under fed and starvation conditions. During starvation, the puncta in CTL had higher intensity of yellow fluorescence than that in *Sac1* RNAi tissues. (I) was the quantification of the yellow:blue ratio of the LysoSensor yellow/blue staining during starvation.  $n = 6$ , \*\*\*,  $p <$

autolysosomes were formed in control tissues (Figure 2P, R). In *Sac1* RNAi animals, electron-dense autolysosomes were enlarged (Figure 2Q, R). The single membrane and electron-dense nature of the autolysosomes in *Sac1* RNAi tissues suggested that the autophagosomes fused with lysosomes successfully. We then knocked down *Syx17* in control and *Sac1* RNAi fat

bodies to examine whether autophagosomes were properly formed upon the loss of *Sac1*. In fed control animals, loss of *Syx17* had little effect and no autophagosome structure was found (Figure 2S); however, the reduction of *Syx17* together with *Sac1* led to the accumulation of autophagosomes in the fat bodies of the fed animals (Figure 2T), suggesting that autophagy was induced in *Sac1* RNAi animals, even without starvation. In starved animals, the loss of *Syx17* led to the accumulation of autophagosomes in both control (Figure 2U) and *Sac1* RNAi animals (Figure 2V), and there were significantly more autophagosomes in *Sac1* RNAi animals than in controls (Figure 2W). These data suggested that reduction in *Sac1* promoted autophagy initiation. However, the autophagy substrates were not fully digested, likely due to the mild increase in autolysosome pH.

#### Levels of PtdIns4P on autolysosomes were critical for autophagy

Since *Sac1* is an ER-localized PtdIns4P phosphatase [33], we examined the distribution of PtdIns4P during starvation. We constructed a transgenic fly carrying a sensitive PtdIns4P reporter, GFP-P4M-SidM [34], which binds to PtdIns4P with high affinity, and expressed it in fat body tissues. GFP-P4M-SidM labeled the cell membrane in both fed and starved animals. In addition, it formed dim small puncta inside cells in the fed animals (Figure 3A) and formed large bright puncta or ring structures colocalized with lysosomes marked with Cp1 in starved animals (Figure 3A'). These bright puncta/rings disappeared if autophagy was blocked by RNAi knock-down of the core autophagy machinery such as *Atg1* (Figure 3B'), *Atg9* (Figure 3C'), or *Atg12* (Figure 3D'). Knockdown of the respective genes in the fat body tissues was confirmed using real-time PCR (Figure S2A). RNAi of *Sac1* slightly increased intracellular GFP-P4M-SidM puncta in fed animals (Figure 3E, M – N'). In starved animals, *Sac1* RNAi dramatically increased intracellular GFP-P4M-SidM puncta, which

colocalized with Cp1 (Figure 3E', M – N'). Overexpression of *Sac1* was largely diffused in the cytosol of both fed and starved animals (Figure 3F, F'). Overexpression of *Sac1* greatly reduced PtdIns4P reporter signals on autolysosomes in starved animals (Figure 3F', M – N'). These data indicated that PtdIns4P was enriched on autolysosomes upon starvation, and the loss of *Sac1* elevated its level.

There are three PtdIns4Ks in flies [35]. We then determined the kinase required for PtdIns4P accumulation on autolysosomes. *fwd* is the ortholog of human *PI4KB*, and RNAi *fwd* reduced the intensity of PtdIns4P reporter signals on the cell membrane in both fed (Figure 3G, M') and starved animals (Figure 3G', M'). In starved animals, the intensity of PtdIns4P reporter signals on lysosomes was also reduced but the distribution pattern was similar to that of the controls (Figure 3G', O). *Pi4KII $\alpha$*  RNAi did not affect PtdIns4P reporter intensity on the cell membrane in both fed (Figure 3H, M') and starved animals (Figure 3H', M'); however, the reduction of *Pi4KII $\alpha$*  decreased the puncta of the PtdIns4P reporter and Cp1 signals inside the starved cells (Figure 3H', M – O'). The reduction in *Pi4KIII $\alpha$*  did not change the intensity of the PtdIns4P reporter in fed animals (Figure 3I, M – N'); however, the reduction of *Pi4KIII $\alpha$*  decreased the intensity of the PtdIns4P reporter in the cytosol of the starved cells (Figure 3I', M – N'). These data suggested that all three PtdIns4Ks contributed to the production of PtdIns4P on lysosomes upon starvation. We also examined key autophagy-related markers in fat bodies with these PtdIns4K reduced (Figure S4). In fed animals, RNAi of any one of the PtdIns4Ks did not change the GFP-RFP-Atg8a patterns (Figure S4A – D). Upon starvation, most Atg8a puncta were red while a few were yellow in the control fat bodies (Figure S4A', E), suggesting that most autophagic structures were acidic. GFP-RFP-Atg8a patterns in *fwd* RNAi (Figure S4B, B', and E) or *Pi4KIII $\alpha$*  RNAi (Figure S4D, D', and E) tissues were similar to those in controls. Almost all the GFP-RFP-Atg8a puncta were yellow in the starved *Pi4KIII $\alpha$*  RNAi fat bodies (Figure S4C', E), indicating that the autophagic structures were not acidic enough to quench GFP signals, likely due to the failure of autophagosome-lysosome fusion, as reported previously [28]. We also examined the expression of the autophagy substrate ref(2)P in *PtdIns4K* RNAi tissues. A slight increase in ref(2)P was observed in all RNAi groups under both fed and starved conditions (Figure S4F – J). The accumulation of ref(2)P

0.001. (J – K'') GFP-*Syx17* labeled autophagosomes were colocalized with lysosome marker Cp1 in both CTL and *Sac1* RNAi tissues upon starvation. The red and green channels of (J') and (K'') were split and shown as gray scale images next to the merged images. The red or green channels were outlined by red or green, respectively. (J'' and K'') were the colocalization curves of green and red signals of the positions marked by short lines in (J' and K'). (L – M'') mCherry-Atg8a labeled autophagosomes and HRP-LAMP1 labeled lysosomes were colocalized in both CTL and *Sac1* RNAi tissues upon starvation. The red and green channels of (L – M') were split and shown as gray scale images next to the merged images. The red or green channels were outlined by red or green, respectively. (L'' and M'') were the colocalization curves of green and red signals of the positions marked by short lines in (L' and M'). (N – V) TEM of the fat bodies in the early third-instar larvae with indicated genotypes. Under fed conditions, there were very few autolysosome-like structures in CTL fat bodies (N). The autolysosome-like structures (red arrows) were occasionally observed in the *Sac1* RNAi tissues (O). (P and Q) Upon starvation, there were more autolysosomes in *Sac1* RNAi fat bodies than that in the CTL tissues. The autophagic structures in the *Sac1* RNAi tissues were electron-dense single membraned structures that resemble mature autolysosomes (Q). (R) were the quantifications of the number and size of the autophagic-structures in the fat bodies with indicated genotypes under either fed or starvation conditions.  $n = 3-5$ , \*,  $p < 0.05$ , \*\*,  $p < 0.01$ . (S – W) Knock-down of *Syx17* in CTL fat bodies led to accumulation of double membraned autophagosomes under starvation (U) but not fed conditions (S). Knock-down of *Syx17* in *Sac1* RNAi fat bodies led to accumulation of autophagosomes in both the fed (T) and starved animals (V). (W) were the quantifications of the numbers of the autophagosomes in the fat bodies with indicated genotypes under either fed or starvation conditions.  $n = 3-4$ , \*,  $p < 0.05$ , \*\*\*,  $p < 0.001$ . The scale bar for the IF images: 10  $\mu\text{m}$ . DAPI marked the nuclei.



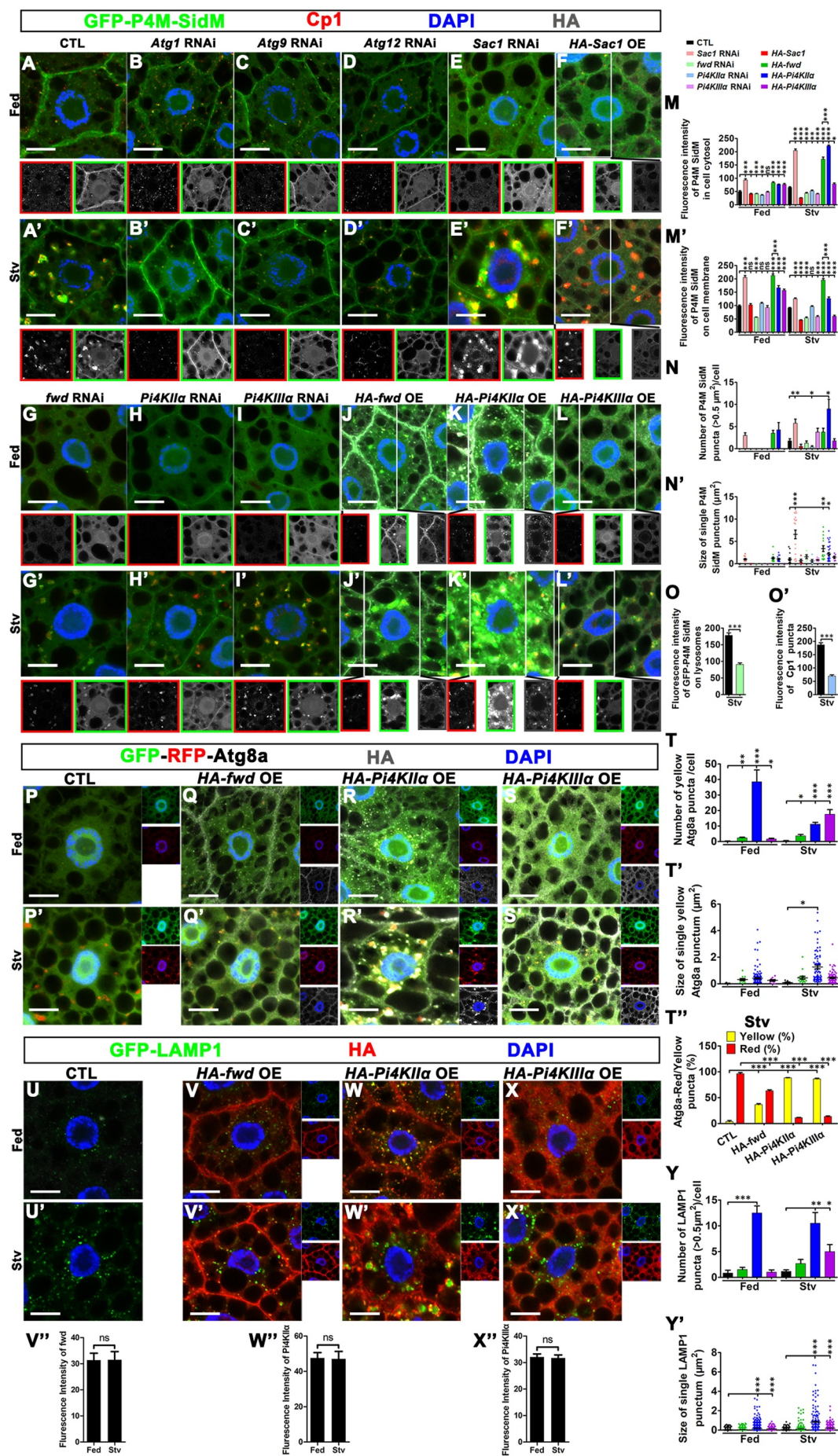


**Figure 3.** Levels of PtdIns4P on autolysosomes were critical for autophagy. The distributions of PtdIns4P in early third-instar larvae fat bodies were analyzed by examining the patterns of PtdIns4P reporter GFP-P4M-SidM. Under fed conditions, GFP-P4M-SidM localized on the cell membrane and form small puncta in the

upon loss of *fwd* under starved conditions was confirmed by driving *fwd* sgRNA and UAS-Cas9 expression in fat body (Figure S4K – M). The GFP-Syx17 and GFP-LAMP1 patterns were also examined. None of the *PtdIns4Ks* RNAi affected the patterns of GFP-Syx17 (Figure S4N – Q) or GFP-LAMP1 (Figure S4S – V) in fed animals. The GFP-Syx17 puncta slightly increased and became elongated to form thin tubular structures in starved *fwd* RNAi fat bodies (Figure S4O', R). *Pi4KIIa* RNAi led to an increase in GFP-Syx17 puncta (Figure S4P', R), whereas *Pi4KIIIa* RNAi did not change GFP-Syx17 patterns in starved animals (Figure S4Q', R). *fwd* RNAi did not change GFP-LAMP1 patterns in starved animals (Figure S4T', W). During starvation, the sizes of GFP-LAMP1 were increased when *Pi4KIIa* was reduced (Figure S4U', W), but those were significantly reduced upon *Pi4KIIIa* reduction (Figure S4V', W). These data suggested that all three *PtdIns4Ks* were required for proper autophagy. The distinct phenotypes observed upon loss of various *PtdIns4Ks* suggested that these kinases regulated autophagy in different manners.

We then expressed HA-tagged *PtdIns4Ks* in the fat body and examined their effects on *PtdIns4P* production and autophagy in fed and starved flies. The majority of HA-Fwd was localized on the plasma membrane and there were small puncta inside the cells (Figure 3J). Starvation did not alter the distribution of Fwd (Figure 3J'). Overexpression of Fwd increased *PtdIns4P* reporter signals in both fed and starved tissues (Figure 3J, J', M–N'). HA-*Pi4KIIa* had both plasma membrane and cytosolic puncta (Figure 3K, K'). The plasma membrane distribution of *Pi4KIIa* was lower than that of Fwd, and cytosolic puncta were more obvious than that of Fwd (Figure 3J, J', K, K', M, and M'). Upon starvation, most *Pi4KIIa* molecules translocated to autolysosomes and formed large puncta (Figure 3K'). Overexpression of HA-*Pi4KIIa* increased cytosolic puncta of the *PtdIns4P* reporter in fed tissues and to a greater extent in starved tissues (Figure 3K, K', M–N'). HA-*Pi4KIIIa* diffused in both fed and starved

tissues (Figure 3L, L'). Overexpression of HA-*Pi4KIIIa* increased the cytosolic *PtdIns4P* reporter signals in both fed and starved animals (Figure 3L, L', M, M'). In the fed animals, *Pi4KIIIa* overexpression increased the *PtdIns4P* reporter signals on the plasma membrane. During starvation, *Pi4KIIIa* overexpression decreased the *PtdIns4P* reporter signals on the plasma membrane (Figure 3L, L', M, M'). Upon starvation, yellow puncta of GFP-RFP-Atg8a and large puncta of GFP-LAMP1 accumulated in *Pi4KIIa* overexpressed tissues (Figure 3R, R', T–T', W, W', Y, Y'). A slight increase of yellow GFP-RFP-Atg8a puncta were also observed but the GFP-LAMP1 pattern did not change when Fwd was overexpressed (Figure 3Q, Q', T–T', V, V', Y, Y'). Overexpression of *Pi4KIIIa* also mildly increased yellow puncta of GFP-RFP-Atg8a and puncta of GFP-LAMP1 upon starvation (Figure 3S–T', X–Y'). The levels of all three *PtdIns4Ks* remained constant under starvation conditions (Figure 3V'–X'). Among three *PtdIns4Ks*, *Pi4KIIa* had most obvious autolysosomal translocation during starvation. Overexpression of *Pi4KIIa* most faithfully phenocopied the loss of *Sac1*. Similar to the results observed in the fat body tissues following knockdown of *Sac1*, the ratio of Atg8a-II:Atg8a-I upon *Pi4KIIa* overexpression increased during starvation (Figure S3B, B'). In addition, overexpression of *Pi4KIIa* in the eyes of developing flies led to degeneration in aged flies (Figure S1G – K). These data suggested that *Pi4KIIa* was a key enzyme in the production of *PtdIns4P* on autolysosomes, and abnormal levels of *PtdIns4P* (too low or too high) on autolysosomes led to autophagy defects.

### ***Osbp* and *cert* were recruited to the autolysosomes by *PtdIns4P* upon starvation**

*PtdIns4P* is a key signaling phospholipid that functions by recruiting downstream effectors. We then investigated the downstream effectors that could be recruited to autolysosomes. We expressed V5 tagged *Osbp*, *cert*, *Arfp*, or HA-tagged *sau*, four molecules that were reported to bind

cytosol in the control fat bodies (A). Upon starvation, GFP-P4M-SidM formed large puncta or ring-like structures colocalized with Cp1 positive autolysosomes (A'). (B – D') Knock-down the expression of key autophagy related molecules, such as Atg1, Atg9, or Atg12, did not change the patterns of GFP-P4M-SidM under fed conditions (B – D), but greatly reduced the formation of large puncta or ring-like structure in the starved animal (B'–D'). (E, E') *Sac1* RNAi increased intracellular GFP-P4M-SidM puncta in both fed and starved animals. (F, F') Overexpressed HA-*Sac1* reduced the GFP-P4M-SidM signals on autolysosomes in starved animals. (G, G') *fwd* RNAi reduced the intensity of GFP-P4M-SidM signals on cell membrane and cytosol in both the fed and starved animals. The distribution pattern of GFP-P4M-SidM signals on lysosomes was similar to the controls. (H, H') *Pi4KIIa* RNAi decreased the intensity of GFP-P4M-SidM in cytosol under both fed and starvation conditions. The size and number of green puncta were also reduced. (I, I') *Pi4KIIIa* RNAi did not change the intensity of GFP-P4M-SidM in the fed cells, but the reduction of *Pi4KIIIa* decreased the intensity of GFP-P4M-SidM in the cytosol of the starved cells and on the membrane of the starved cells. (J – L') HA tagged *PtdIns4Ks* were expressed in fat body and their expression patterns (gray) were examined together with the expression of GFP-P4M-SidM (green). (J, J') Majority of HA-Fwd localized on the plasma membrane and a small amount of HA-Fwd formed puncta inside cells in both fed and starved animals. The overexpression of Fwd increased the intensity of GFP-P4M-SidM in both fed and starved tissues. (K, K') HA-*Pi4KIIa* had both plasma membrane and cytosolic puncta distributions. During starvation, *Pi4KIIa* translocated on the autolysosomes (red) and formed large puncta. The overexpression of HA-*Pi4KIIa* increased sizes and numbers of cytosolic puncta of GFP-P4M-SidM in both fed and the starved tissues. (L, L') HA-*Pi4KIIIa* was diffused in both fed and starved tissues. The overexpression of HA-*Pi4KIIIa* slightly increased the intensity of GFP-P4M-SidM in cytosol but did not affect its patterns in both fed and starved tissues. The red, green or gray channels of (A – L') were split and shown as gray scale images at the bottom of the merged images. The red, green, or gray channels were outlined by red, green, or gray, respectively. For image (F, F', J – L'), only the boxed regions in the merged images were shown in the split channels. (M – O') the statistics of the fluorescence intensity and patterns of GFP-P4M-SidM in the tissues with indicated genotypes under either fed or starved conditions.  $n = 4$ , ns: not significant, \*:  $p < 0.05$ , \*\*:  $p < 0.01$ , \*\*\*:  $p < 0.001$ . (P – Y') HA-tagged *PtdIns4Ks* were overexpressed in fly fat bodies and the signals of GFP-RFP-Atg8a or GFP-LAMP1 were examined in the early third-instar larvae under fed and starvation conditions. (P – T') the numbers of yellow puncta of GFP-RFP-Atg8a increased when the *PtdIns4Ks* were overexpressed. The overexpression of HA-*Pi4KIIa* dramatically increased yellow GFP-RFP-Atg8a puncta. (T – T') were the statistics of the GFP-RFP-Atg8a puncta in the fat body cells with indicated genotypes under fed and starvation conditions.  $n = 4$ , \*:  $p < 0.05$ , \*\*:  $p < 0.01$ , \*\*\*:  $p < 0.001$ . (U – X) the overexpression of HA-*Pi4KIIa* dramatically increased GFP-LAMP1 puncta in both fed and starvation condition. The overexpression of HA-*Pi4KIIIa* increased GFP-LAMP1 puncta under both fed and starvation conditions. (V'–X') were the statistical data of the intensity of fluorescence signals for each *PtdIns4Ks* in fat bodies of the animals under fed or starvation conditions.  $n = 7$ ; ns: not significant. (Y, Y') were the statistics of the GFP-LAMP1 puncta in the fat body cells with indicated genotypes under fed and starvation conditions.  $n = 4$ , \*:  $p < 0.05$ , \*\*:  $p < 0.01$ , \*\*\*:  $p < 0.001$ . Scale bar: 10  $\mu\text{m}$ . DAPI marked the nuclei.



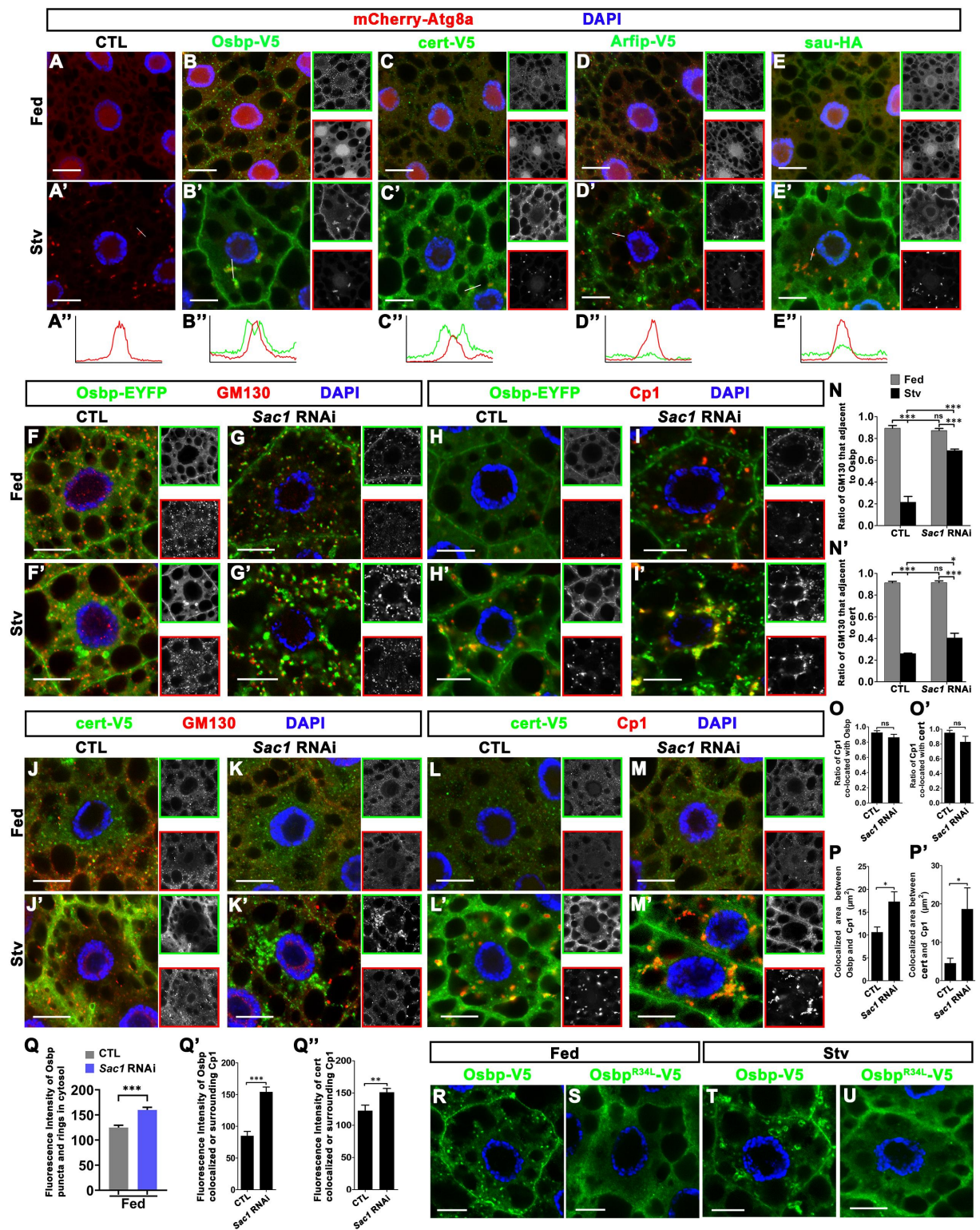


**Figure 4.** Osbp and cert were recruited to the autolysosomes by PtdIns4P. (A – E'') V5 or HA tagged PtdIns4P binding proteins were expressed together with mCherry-Atg8a in early third instar larvae fat bodies. During starvation, Osbp and cert, but not Arfp or sau, was recruited to the mCherry-Atg8a positive autolysosomes. (A''–E'') were the colocalization curves of green and red signals of the positions marked by short lines in (A'–E'). (F – I') Osbp-EYFP formed small puncta that were adjacent to Golgi marker GM130 in cytosol under fed conditions in both CTL and *Sac1* RNAi tissues. During starvation, Osbp-EYFP formed large puncta or ring-like structures that colocalized with Cp1. Some small Osbp-EYFP puncta were still adjacent GM130 in *Sac1* RNAi tissues. (J – M') cert-V5 formed small puncta that were adjacent to Golgi marker GM130 in cytosol under fed conditions in both CTL and *Sac1* RNAi tissues. (J'–M') During starvation, cert-V5 formed large puncta or ring-like structures that surrounded or colocalized with Cp1. A fraction of cytosolic cert puncta was near the GM130 puncta in *Sac1* RNAi tissues. The red or green channels of (A – M') were split and shown as gray scale images next to the merged images. The red or green channels were outlined by red or green, respectively. (N, N') the ratio of GM130 that adjacent to Osbp (N) or cert (N') was quantified in control or *Sac1* RNAi tissues under fed or starvation conditions.  $n = 3$ , \*,  $p < 0.05$ , \*\*\*,  $p < 0.001$ , ns: not significant. (O, O') the ratio of Cp1 that co-localized with Osbp (O) or cert (O') was quantified in control or *Sac1* RNAi tissues under

to PtdIns4P, together with mCherry-Atg8a in the fat body, and we subsequently examined their patterns in fed and starved animals (Figure 4A–E’). Upon starvation, Osbp and cert, but not Arfp or sau, were recruited to autolysosomes labeled with mCherry-Atg8a (Figure 4A–E’), suggesting that Osbp and cert could be effectors that mediate PtdIns4P function on the autolysosomes.

We then examined whether the loss of *Sac1* led to the recruitment of more Osbp or cert to the lysosomes. Since Osbp and cert were reported to be localized on the Golgi apparatus, we examined the distribution of Osbp and cert in the wild-type or *Sac1* RNAi tissues by co-staining with the Golgi marker GM130 (Golgi matrix protein 130 kD) or lysosome marker Cp1 (Figure 4F–Q’). Under fed conditions, cytosolic Osbp puncta (Figure 4F, G) or cert (Figure 4J, K) were small and adjacent to GM130 in both wild-type and *Sac1* RNAi tissues, indicating that Osbp and cert were localized in the Golgi apparatus. *Sac1* RNAi slightly increased the signal intensity of Osbp puncta in the cytosol (Figure 4G, I, Q), but did not change the patterns of cert (Figure 4K, M) in fed animals. Upon starvation, Osbp and cert formed large puncta or ring-like structures surrounding Cp1, and their association with GM130 was greatly reduced in wild-type tissues (Figure 4F’, J’, N, and N’). In *Sac1* RNAi tissues, starvation increased the intensity of Osbp puncta and rings inside the cytosol (Figure 4G’, I’, N, O, P, and Q’). Small Osbp puncta were near GM130 (Figure 4G’, N) and large puncta/ring-decorated Cp1-labeled autolysosomes (Figure 4I’, O, P, and Q’). In starved *Sac1* RNAi tissues, cytosolic cert increased dramatically. Most cytosolic cert was co-localized with Cp1 (Figure 4K’, M’, N’, O’, and P’). The fluorescence intensities of both Osbp and cert co-localized with Cp1 were increased in starved *Sac1* RNAi tissues compared to those in starved controls (Figure 4Q’, Q’’).

We then examined whether Osbp puncta formation depended on PtdIns4P level. We expressed a mutant form of Osbp (Osbp<sup>R34L</sup>) that carried a point mutation in its PH domain and could not bind PtdIns4P in the fat body. Osbp<sup>R34L</sup> diffused inside cells and could not form puncta or ring-like structures in cells (Figure 4S, U), as its wild type (Figure 4R, T) did under both fed and starvation conditions.

### Osbp and cert were required for autophagy

Since Osbp and cert could be recruited to autolysosomes, we wondered whether they were required for autophagy. We reduced *Osbp* or *cert* expression levels in the fat bodies and analyzed different autophagy markers. The reduction in Osbp

levels did not significantly change the patterns of mCherry-Atg8a and GFP-RFP-Atg8a under both fed and starvation conditions (Figure 5a–b’, m–n’, Figure S5A, A’, G). *Osbp* sgRNA and Cas9 expression dramatically increased the puncta of GFP-Atg9 (Figure 5c–d’, Figure S5B, B’), GFP-FYVE (Figure 5e–f’, Figure S5C, C’), GFP-LAMP1 (Figure 5k–l’, Figure S5F, F’), and HA-ref(2)P (Figure 5o–p’, Figure S5H, H’) under both fed and starved conditions. The puncta of GFP-Rab7 and GFP-Syx17 did not change under fed conditions (Figure 5g, h, i, and j, Figure S5D, D’), but significantly increased upon starvation when *Osbp* was reduced (Figure 5g’, h’, i’, and j’, Figure S5D – E’). We also examined the expression of Atg8a in the fat bodies using western blotting. The Atg8a-II:Atg8a-I ratio did not change significantly in tissues with reduced *Osbp* under both fed and starved conditions (Figure S3C, C’). However, in tissues with reduced *Osbp*, the total levels of Atg8a were decreased compared to those in the control tissues (Figure S3C, C’).

We also knocked down *cert* expression in fly fat bodies and found an increase in the puncta of mCherry-Atg8a (Figure 5A–B’, Figure S5I, I’), GFP-Atg9 (Figure 5C–D’, Figure S5J, J’), GFP-FYVE (Figure 5E–F’, Figure S5K, K’), GFP-Rab7 (Figure 5G–H’, Figure S5L, L’), GFP-Syx17 (Figure 5I–J’, Figure S5M, M’), or GFP-LAMP1 (Figure 5K–L’, Figure S5N, N’) upon starvation. GFP-RFP-Atg8a formed yellow puncta in starved tissues with *cert* RNAi (Figure 5M–N’, Figure S5O), suggesting a block of autophagy flux. In addition, a slight increase in HA-ref(2)P was observed in *cert* RNAi tissues (Figure 5O–P’, Figure S5P, P’). Similar to the observation of *Sac1* RNAi in the fat bodies, the Atg8a-II:Atg8a-I ratio increased significantly in tissues with reduced *cert* under starvation conditions (Figure S3D, D’). Overall, the changes in autophagy markers in tissues with *Osbp* or *cert* reduction were similar but less obvious than the changes in *Sac1* RNAi tissues.

### Osbp and cert were required for neuronal homeostasis

The reduction in Osbp and cert mimicked the autophagy defects that were observed when *Sac1* was reduced. We then investigated whether the reduction in Osbp or cert also affects neuronal homeostasis. We used GMR-Gal4 to drive *cert* siRNA expression in the fly eyes and examined the retinal morphology in the 2-day and 31-day old animals by TEM. The reduction of *cert* in fly eyes caused degeneration in the retina of 31-day old flies (Figure 6A–D’, G). Co-expression of cert and *cert* siRNA rescued the eye degeneration phenotypes (Figure 6E–F’, G). We also used GMR-Gal4 driving UAS-Cas9 and *Osbp* sgRNA expression in developing fly eyes and

---

starvation conditions.  $n = 5$ , ns: not significant. (P, P’) the areas of Osbp (P) or cert (P’) that co-localized with Cp1 were quantified for control or *Sac1* RNAi tissues under starvation conditions.  $n = 4$ , \*,  $p < 0.05$ . (Q) was the quantification of the fluorescence intensity of Osbp puncta in the fat body cells with indicated genotypes under fed conditions.  $n = 6$ , \*\*\*,  $p < 0.001$ . (Q’, Q’’) were the quantification of the fluorescence intensity of the Osbp (Q’) or cert (Q’’) puncta that co-localized with Cp1 under starvation conditions.  $n = 10$ , \*\*,  $p < 0.01$ , \*\*\*,  $p < 0.001$ . (R – U) V5 tagged Osbp or Osbp<sup>R34L</sup> (a PH domain mutant form) were expressed in fat bodies. Osbp<sup>R34L</sup> lost the cytosolic puncta patterns in both fed and starved animals. Scale bar: 10  $\mu$ m. DAPI marked the nuclei.



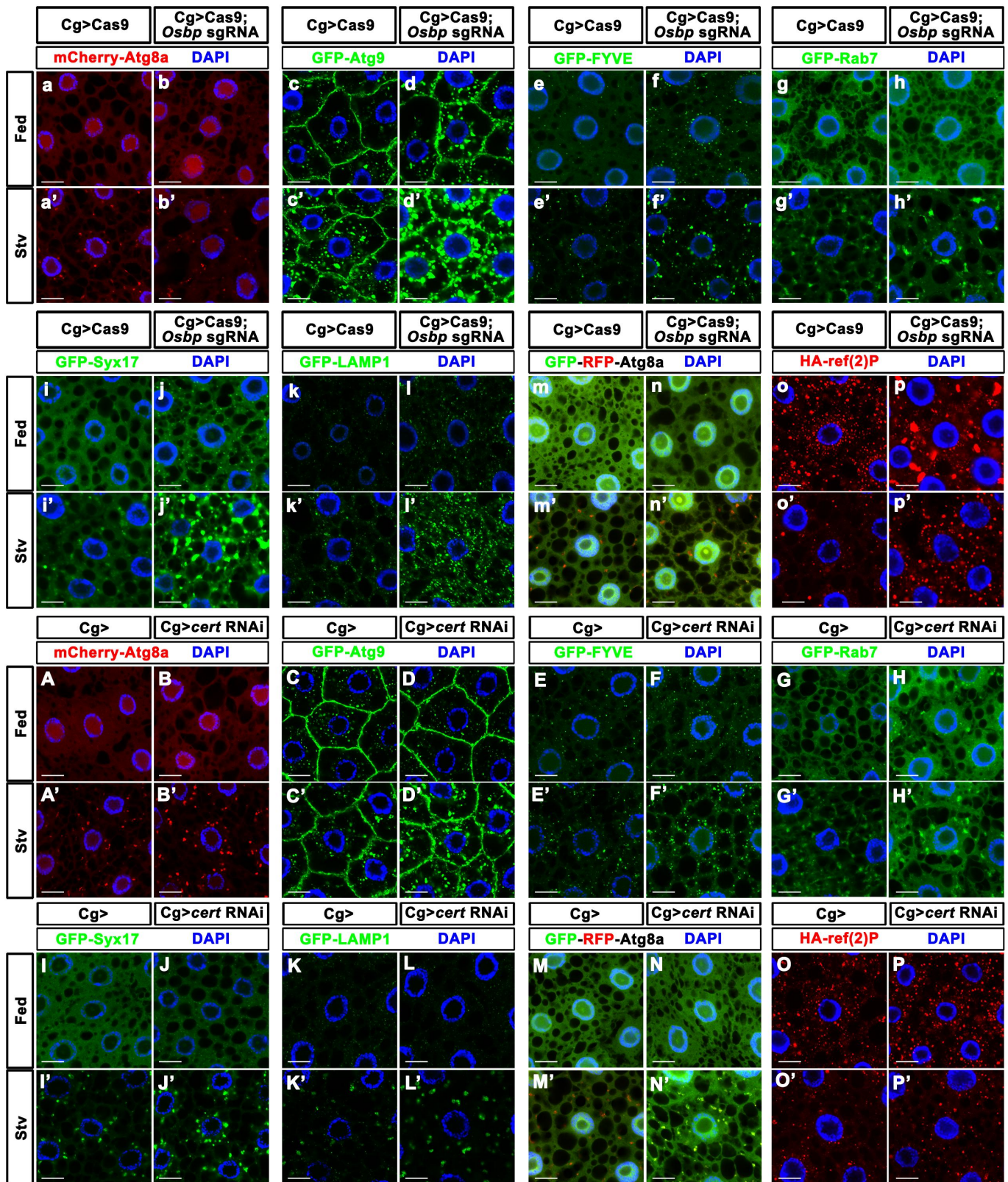


**Figure 5.** Cert and *Osbp* were required for autophagy. Autophagy markers were analyzed in the fat bodies of the animals with indicated genotypes under fed and starvation conditions. (a – b') mCherry-Atg8a patterns did not change in the tissues with reduced *Osbp* (b, b') expression under both fed (a, b) and starvation (a', b') conditions. (c – d') Reduction of *Osbp* expression increased GFP-Atg9 puncta under both fed (c, d) and starvation (c', d') conditions. (e – f') Reduction of *Osbp* expression increased GFP-FYVE puncta under both fed (e, f) and starvation (e', f') conditions. (g – h') Reduction of *Osbp* expression did not change GFP-Rab7 patterns under fed conditions (g, h), but increased the puncta of GFP-Rab7 during starvation (g', h'). (i – j') Reduction of *Osbp* expression did not change the patterns of GFP-Syx17 under fed condition (i, j), but increased the puncta of GFP-Syx17 during starvation (i', j'). (k – l') Under both fed and starvation conditions, GFP-LAMP1 puncta increased in the tissues with reduced *Osbp* expression. (m – n') the patterns of GFP-RFP-Atg8a did not change in the tissues with reduced *Osbp* expression under both fed (m, n) and starvation (m', n') conditions. (o – p') Under both fed (o, p) and starvation (o', p') conditions, HA-ref(2)P puncta increased in the tissues with reduced *Osbp* expression. (A – B') in *cert* RNAi tissues, the patterns of mCherry-Atg8a did not change under fed conditions (A, B), but increased during starvation (A', B'). (C, D) *cert* RNAi slightly increased puncta size of Atg9, but did not change the number of GFP-Atg9 puncta under fed conditions. (C', D') *cert* RNAi increased both

examined eye morphology in 2-day and 31-day old flies. In 2-day old flies, small fractions of PRs were missing from the ommatidia. In 31-day old flies, the loss of *Osbp* led to the loss of PRs in most of the ommatidia, indicating the degeneration of PRs (Figure 6H–L). These data suggested that both *Osbp* and *cert* were required for neuronal homeostasis.

### **Sac1 facilitated PtdIns4P exchange by *Osbp* and *cert* at the ER-autolysosome contacts**

*Osbp* and *cert* have been reported to function at ER-Golgi contacts to transport cholesterol and ceramides from the ER to the Golgi apparatus, respectively. As an exchange, *Osbp* could transport PtdIns4P from the Golgi to the ER, followed by dephosphorylation of PtdIns4P by ER-localized *Sac1* [23]. As *Osbp* and *cert* could be recruited to the autolysosome during autophagy, we wondered whether *Osbp* and *cert* could transport cholesterol and ceramides to autolysosomes, respectively. We knocked down *Osbp* and *Sac1* in early third-instar larvae fat bodies and stained cholesterol with filipin in the fed and starved animals (Figure 7A–F, M). Filipin staining diffused in the fed animals (Figure 7A, A'). Upon starvation, the GFP-LAMP1 labeled autolysosomes were also stained with filipin (Figure 7B, B'), suggesting cholesterol enrichment in the autolysosomes. Loss of *Osbp* led to an increase in the cytosolic levels of filipin staining in both fed and starved tissues (Figure 7C–D, M). Filipin staining of autolysosomes in starved animals with reduced *Osbp* was more obvious than that in starved control animals (Figure 7B, B', D, and D'). Knockdown of *Sac1* also slightly increased the cytosolic level of filipin staining in the fed animals (Figure 7E, E', M). In starved *Sac1* RNAi animals, the filipin signals on the autolysosomes were significantly increased compared to the control animals (Figure 7F, F', M).

We also used an anti-ceramide antibody to stain fat body tissues with reduction of *cert* or *Sac1* (Figure 7G–M). In the control animals, the ceramides were mainly localized on the plasma membrane under both fed and starved conditions (Figure 7G–H'). Ceramide was not enriched in the autolysosomes (Figure 7H, H'). The reduction in *cert* in the fed animals did not change the ceramide pattern; however, the loss of *cert* led to a dramatic increase in ceramides in the plasma membrane and cytosol in starved animals (Figure 7I–J', M). Cytosolic ceramide puncta did not colocalize with the autolysosomes (Figure 7J, J'). The loss of *Sac1* did not change the patterns of ceramide, but slightly increased its levels under both fed and starved conditions (Figure 7K–M).

We investigated whether PtdIns4P was transported by *Osbp* and *cert*. The reduction of *cert* and *Osbp* greatly

increased PtdIns4P levels on the autolysosomes in the starved animals (Figure 7N–P', R), suggesting that both proteins were required for the transport and dephosphorylation of PtdIns4P. *Osbp* and *cert* transport PtdIns4P, cholesterol, or ceramides through ER-Golgi contacts mediated by VAP proteins [23,36]. We investigated whether VAP protein (*Vap33* in *Drosophila*) was required for PtdIns4P transport at ER-autolysosome contacts. We knocked down *Vap33* expression in fat bodies and examined the patterns of the PtdIns4P reporter in both fed and starved animals. The reduction in *Vap33* increased cytosolic PtdIns4P puncta in both fed and starved animals (Figure 7Q–R). We then examined whether ER-autolysosome contacts were present during starvation. The contacts were defined as 10–30 nm intervals between the rough ER and single-membrane autolysosome structures. At the contact sites, ribosomes were absent from the ER surface facing autolysosomes. We examined the fat bodies of early third-instar larvae under starvation conditions using TEM. We observed a few cases in which autolysosomes were in close contact with ER (Figure 7T, T', Z''); however, most autolysosomes in starved animals did not contact the ER (Figure 7S, S', Z''), likely because the contacts between these two organelles were transient. Interestingly, in *Sac1* RNAi tissues, the contacts were frequently observed upon starvation (Figure 7U–V', Z''). This suggested that the blockage of PtdIns4P dephosphorylation by *Sac1* blocked the dissociation of the contacts between the ER and autolysosomes. We then investigated whether *Osbp* mediated the contact between autolysosomes and the ER. We overexpressed *Osbp* in the fat bodies and observed an increase in contacts (Figure 7W–X', Z''). We also overexpressed a mutant form of *Osbp* (*Osbp*<sup>CBmu (H503A H504A K713A)</sup>) that cannot transfer cholesterol but is still able to bind to PtdIns4P and *Vap33*. When *Osbp*<sup>CBmu</sup> was overexpressed, most autolysosomes were wrapped by the ER (Figure 7Y–Z''), suggesting a significant increase in ER-autolysosome contacts. The increase in contacts was more dramatic in the tissues with *Osbp*<sup>CBmu</sup> overexpression than in the tissues with *Osbp* overexpression (Figure 7Z''), which was likely because *Osbp* but not *Osbp*<sup>CBmu</sup> overexpression triggered the reduction of PtdIns4P, which released *Osbp* from autolysosomes and led to the disassemble of the contacts.

## **Discussion**

Contact between the ER and other organelles is critical for many cellular events [1]. In this study, we found that PtdIns4P and its effectors mediated contacts between the ER and autolysosomes. These contacts might facilitate

---

the size and number of GFP-Atg9 puncta under starvation conditions. (E – F') *cert* RNAi did not change GFP-FYVE patterns under fed conditions (E, F), but increased GFP-FYVE puncta under starvation (E', F') conditions. (G – H') *cert* RNAi did not change GFP-Rab7 patterns under fed conditions (G, H), but increased the puncta of GFP-Rab7 during starvation (G', H'). (I – J') Reduction of *cert* expression did not change the patterns of GFP-Syx17 under fed condition (I, J), but increased the puncta of GFP-Syx17 during starvation (I', J'). (K – L) Under fed conditions, *cert* RNAi slightly increased GFP-LAMP1 puncta size. (K', L') Under starvation conditions, GFP-LAMP1 puncta increased in the tissues with reduced *cert* expression. (M – N) The patterns of GFP-RFP-Atg8a did not change in the tissues with reduced *cert* expression under fed conditions. (M', N') the yellow puncta were greatly increased in the *cert* RNAi tissues under starvation conditions. (O – P') Under both fed (O, P) and starvation (O', P') conditions, HA-ref(2)P puncta increased in the tissues with reduced *cert* expression. Scale bar: 10  $\mu$ m. DAPI marked the nuclei.



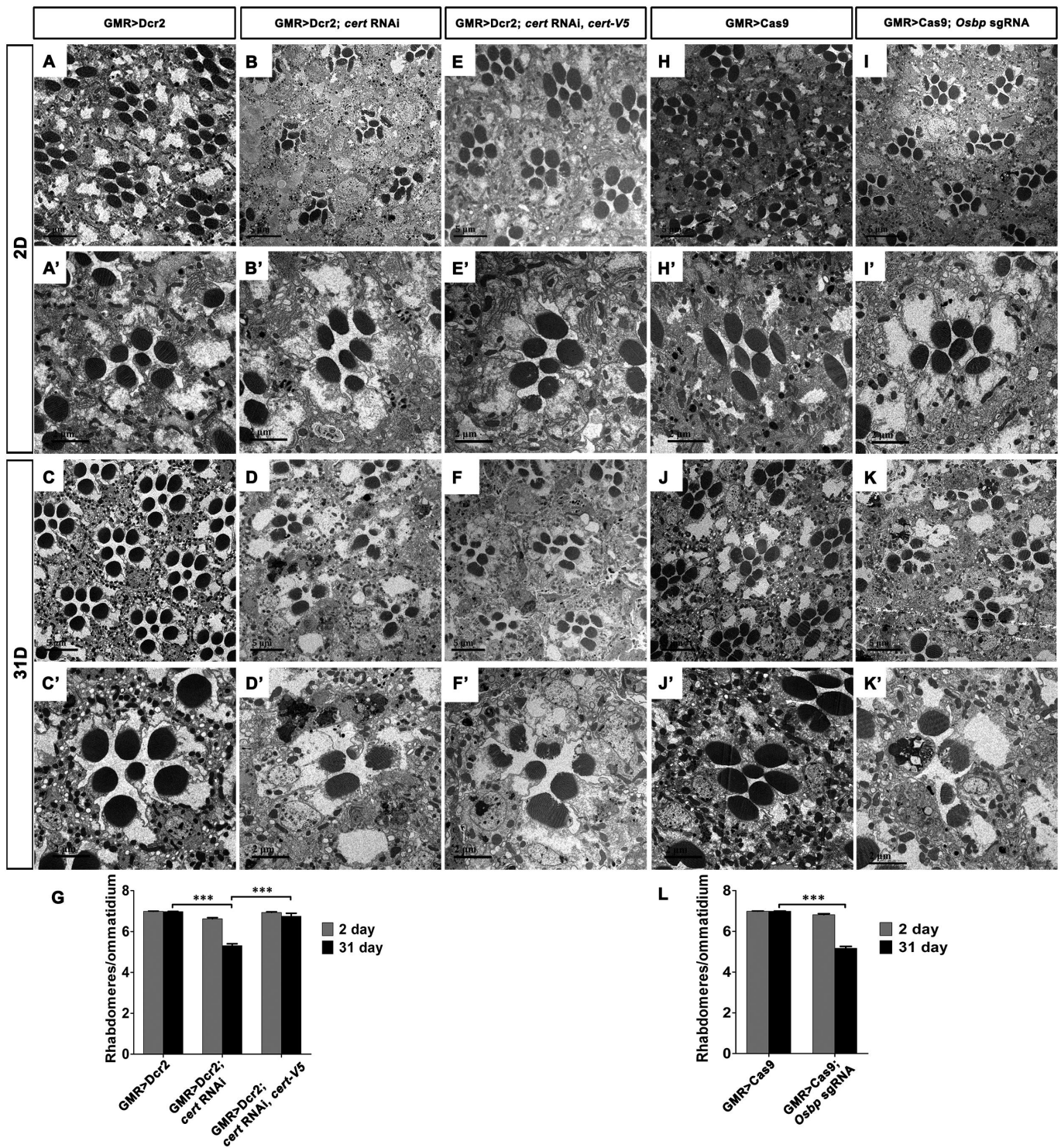


**Figure 6.** *Cert* and *Osbp* were required for neuronal homeostasis in fly eyes. TEM analyses were performed for the retina from young (2 days (2D)) or old (31 days (31D)) flies with indicated genotypes. (A – K) were large views to show the morphology of the retina and (A'–K') were small views to show the detailed structures of individual ommatidium. (B') the autophagosome/autolysosome-like structures could occasionally be found in the glial cells when *cert* was reduced in the eye. In the 31D flies, the ommatidia were intact in the control (*GMR>Dcr2*) flies (C, C'). The numbers of rhabdomeres were progressively reduced in *cert RNAi* flies (D and D'). (E – F') the degeneration of PRs in *cert RNAi* eyes was largely rescued by overexpression of *cert*. (H – K') the numbers of rhabdomeres were progressively reduced in the eyes with reduced *Osbp* (K, K') but not controls (J and J'). (G and L) were the statistics of the average number of rhabdomeres per ommatidia in the animals with indicated genotypes.  $n = 16\text{--}50$ , \*\*\*:  $p < 0.001$ .

cholesterol (or other lipids) transport from the ER to the autolysosomes; simultaneously, PtdIns4P was transported from the autolysosome to the ER, where it underwent hydrolysis by *Sac1*. This type of contact borrowed the entire set of

machinery on the contacts between the ER and Golgi apparatus. Both types of contacts used PtdIns4P not only as a signal molecule to recruit effectors, such as *Osbp* and *cert*, to establish contacts but also as “fuels” hydrolyzed by *Sac1* to



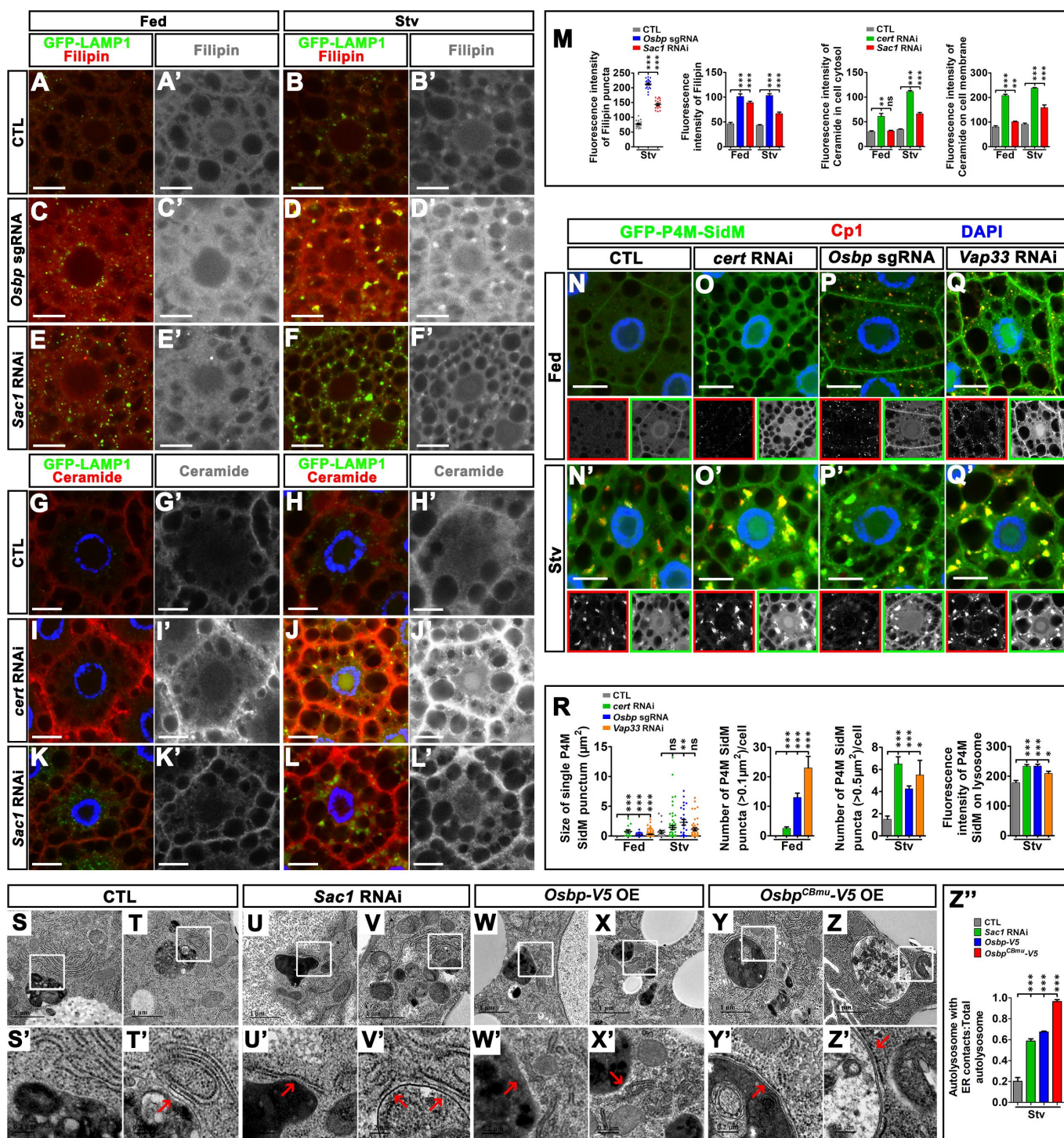


**Figure 7.** *Sac1* facilitated PtdIns4P exchange by *Osbp* and *cert* at the ER-autolysosome contacts. (A – F) Filipin staining (red) was performed for the early third-instar larvae fat bodies under fed or starvation conditions. Lysosomes and autolysosomes were labeled by GFP-LAMP1. (A'–F') indicated the red channels (signals of filipin) of (A – F). (A, A') Filipin signals were diffused in the control tissues under fed conditions. (B, B') Filipin signals were enriched on the GFP-LAMP1 (green) positive autolysosomes during starvation. (C – D') Reduction of *Osbp* increased the basal level of filipin staining in the cytosol under both fed and starvation conditions. The intensity of filipin on the autolysosomes was increased (D, D'). (E, E') *Sac1* RNAi increased the basal level of filipin signals in the cytosol under fed conditions. (F, F') During starvation, *Sac1* RNAi increased the intensity of filipin both on the autolysosomes and in the cytosol. (G – L') Ceramide (red) was indicated by anti-ceramide staining for the early third-instar larvae fat bodies under fed and starvation conditions. Lysosomes and autolysosomes were labeled by GFP-LAMP1. (G – H') Ceramide was diffused in the fat body cells and was enriched on the plasma membrane under both fed and starvation conditions. (I – J') *cert* RNAi increased the basal level of ceramide in cells under both fed and starvation conditions. There were some puncta staining of ceramide in the cytosol under starvation conditions (J, J'). However, the puncta were not specifically associated with autolysosomes labeled with GFP-LAMP1. (K – L') *Sac1* RNAi increased ceramide levels in the fat bodies under both fed and starvation conditions. (M) were the statistics for the signals of filipin or ceramide in the tissues with indicated genotypes under either fed or starvation conditions.  $n = 4$ , ns: not significant, \*\*:  $p < 0.01$ , \*\*\*:  $p < 0.001$ . (N – R) the patterns of PtdIns4P reporter GFP-P4M-SidM were analyzed in the early third-instar larval fat bodies in the animals with indicated genotypes. Lysosomes/autolysosomes were labeled with Cp1 (red). The puncta of GFP-P4M-SidM were increased in the fat bodies with reduction of the expression of *cert*, *Osbp*, or *Vap33* under both fed and starvation conditions. The red or green channels of (N – Q') were split and shown as gray scale images at the bottom of the merged images. The red or green channels were outlined by red or green, respectively. (R) were the statistics for the signals of GFP-P4M-SidM in the animals with indicated genotypes under either fed or starvation conditions.  $n = 4$ , ns: not significant, \*:  $p < 0.05$ , \*\*:  $p < 0.01$ , \*\*\*:  $p < 0.001$ . (S



trigger lipid transfer and regulate the dynamics of the contacts. The contacts between the ER and autolysosomes were very dynamic and rarely observed in wild-type tissues upon autophagy. These contacts were transient, likely because PtdIns4P effectors, such as *Osbp*, no longer mediated membrane tethering when PtdIns4P was decreased on the surface of autolysosomes. Loss of *Sac1* blocked lipid transfer and locked the two organelles at the contact positions (Figure 8).

We did not have direct evidence to show the exact direction of the lipid (such as cholesterol) transport. According to the model we proposed, cholesterol level should decrease on the autolysosomal membrane in the tissues with reduced *Sac1* or *Osbp*. Instead, we observed autolysosomes with increased filipin staining in those tissues. The discordance might be due to that we could not distinguish cholesterol on the autolysosomal membrane from cholesterol inside the autolysosome by filipin staining. Cholesterol is enriched in the autophagy cargos and therefore its level will increase if the autophagy cargo failed to be fully digested, which is what happened in the tissues with reduced *Sac1* or *Osbp*. The cytosolic levels of cholesterol or ceramide increased in the tissues with reduced *Sac1* or *Osbp/cert*, which may reflect the increase of these lipids in ER because of the dampened transport processes. The transport of the lipids other than PtdIns4P between ER-autolysosomal contacts was still speculation at this point. Further studies are required to elucidate which lipid is transported and in what direction it is transported.

Before this study, contacts between the ER and lysosomes were observed under normal culture conditions. The lysosomal lipid transfer protein ORP1L mediates contacts between the ER and endolysosomes to coordinate cholesterol transfer with the retrograde movement of endolysosomal vesicles [37]. NPC1 (Niemann-Pick type C protein 1) was also reported to interact with the sterol transport protein GRAMD1B to tether ER and endocytic organelles and regulate cholesterol egress [38]. OSBP delivers cholesterol across ER-lysosome contacts to activate MTORC1 [39]. In addition, the SNX13 (sorting nexin 13) protein has also been reported as a negative regulator of lysosomal cholesterol export and contributes to ER-lysosome membrane contact sites [40]. These studies all support the idea that the ER and lysosomes have active cholesterol exchange and that several molecules are involved. In this study, we determined that, during autophagy, the relocalization of Pi4KII $\alpha$  from the Golgi apparatus to autolysosomes helped to relocate the entire machinery from ER-Golgi contacts to ER-autolysosome contacts. Our data suggested that both *Osbp* and *cert* functioned in ER-autolysosome contacts. The composition of cholesterol and other lipids in the autolysosome might regulate MTOR activity and V-ATPase assembly, which might explain why the pH of the autolysosome in *Sac1* RNAi tissues was increased.

Our study revealed no defects in autophagosome-lysosome fusion, although the cargos failed to be fully digested in the autolysosomes of *Sac1* mutant flies. However, loss of *Sac1* leads to autophagosome-lysosome fusion defects during autophagy in yeast and xenophagy in mammalian cells [22,41]. Our results suggested that *Sac1* facilitated lipid exchange between the ER and autolysosomes and promoted autolysosome acidification. It remained unclear whether the contacts formed before or after autophagosome-lysosome fusion. Detailed analysis is required to identify the step at which contacts are formed during autophagy. Recruitment of PI4KII $\alpha$  to autophagosomes and increased PtdIns4P levels on autolysosomes have also been observed in mammals, suggesting that our models are at least partially conserved in higher organisms. The lipid composition of the autophagic membrane might affect membrane fusion, autolysosome acidification, and other properties of autophagosome structures in an organism- or context-specific manner. "Descent with modification" is the theme of evolution, and thus subtle differences are expected to exist in different organisms. We do not think *Sac1*'s functions in autophagy change from yeast to *Drosophila* and change back from *Drosophila* to mammals. The subtle modification of *Sac1*'s function could happen long after *Drosophila* went into a separate path from other species in the long journey of evolution.

We observed an increase in PtdIns4P on autolysosomes in the tissues with a reduction in *cert* upon starvation. This suggested that *cert* functioned on autolysosomes to transport PtdIns4P; however, we did not observe an obvious accumulation of ceramide on the autolysosome upon starvation. It is possible that ceramide was not transported between autolysosomes and the ER. Alternatively, the current antibody was not sensitive enough to detect a small amount of ceramide transported at ER-autolysosome contacts. We found that the reduction in *cert* resulted in the accumulation of ceramide in the fat body under fed conditions and was more dramatic under starvation conditions. This suggested that ceramide transport was actively regulated by starvation, and *cert* was required for ceramide transport. A slight increase in ceramide levels in tissues with *Sac1* knockdown suggested that *Sac1* participated in ceramide transport. However, it is unclear whether ceramide transport is required for starvation-induced autophagy. ORD domain-containing proteins can transfer phospholipids other than cholesterol. Further experiments are needed to determine whether *Osbp* and *cert* can transport other lipids using PtdIns4P as a "fuel".

In our study, the loss of either *Osbp* or *cert* led to autophagy defects and neurodegeneration; however, neither phenotype fully mimicked the loss of *Sac1* expression. Considering that all these proteins are multifunctional, we do not think that the degeneration was completely due to

– Z') the TEM of the fat body tissues from the animals with indicated genotypes under starvation conditions. Two independent images for each genotype were shown. The ER-autolysosome contacts were indicated by red arrows. (S' – Z') were the enlarged views of the boxed regions in (S – Z). In control (CTL) tissues, ER-autolysosome contacts were occasionally been observed (T, T'). *Sac1* RNAi, overexpression of V5 tagged *Osbp* or *Osbp*<sup>CBmu</sup> increased the ER-autolysosome contacts. (Z'') were the statistics of the ratio of autolysosomes with ER-autolysosome contacts vs total autolysosomes.  $n = 3$ , \*\*\*:  $p < 0.001$ . The scale bar for the IF images: 10  $\mu$ m. DAPI marked the nuclei.

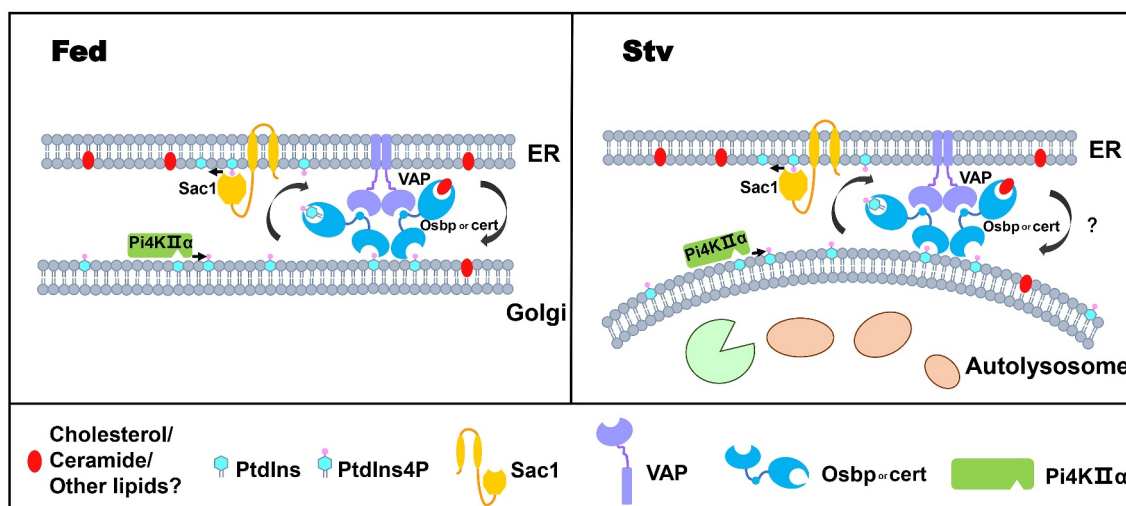


**Figure 8.** The working model. A same set of molecular machinery was used by two distinct organelle contacts under different nutrition statuses. Under fed conditions, PtdIns4P recruited its effectors Osbp and cert to the Golgi apparatus. The interaction between Osbp and ER protein VAP mediated ER-Golgi contact. PtdIns4P was transported from the Golgi apparatus to ER and hydrolyzed by Sac1, which triggered the cholesterol or other lipid transfer between two organelles mediated by Osbp and cert. During starvation, Pi4KII $\alpha$  transferred from Golgi to autolysosomes and produced PtdIns4P on the surface of autolysosomes. Osbp and cert proteins were recruited by the autolysosomal PtdIns4P and established contacts between ER and autolysosomes, which might facilitate lipid such as cholesterol transfer from ER to the membrane of autolysosomes. The defects in PtdIns4P hydrolyzation resulted in abnormal autophagy and neuronal death.

the malfunction of autophagy. We have no direct evidence that the malfunction of autophagy in these animals led to neurodegeneration. It would not be surprised that autophagy defects contribute to the degeneration in those animals considering the important functions of autophagy in maintaining neuronal homeostasis.

It is puzzling that mCherry-Atg8a or GFP-RFP-Atg8a did not show defects upon the reduction of Osbp. It suggests that Osbp may function differently from Sac1 and cert in the autophagy steps such as initiation. Another possible explanation is that mCherry-Atg8a and GFP-RFP-Atg8a may not be sensitive enough to detect the defects in the tissues with reduced Osbp. We think cert and Osbp probably not function in a linear pathway with Sac1. Loss of Sac1, cert, Osbp, or Vap33 led to increased PtdIns4P on autolysosomes, but their roles differed. Vap33 served as a tether to mediate contact. cert and Osbp interacted with Vap33 and served as tethers. Both proteins transferred PtdIns4P from the autolysosome to the ER while transferring other lipids to the autolysosome. Sac1 hydrolyzed PtdIns4P in the ER. Therefore, loss of Sac1 or Vap33 led to reductions in lipids (cholesterol, ceramide or other unknown lipids) as well as increased PtdIns4P on autolysosome membrane. However, loss of Osbp or cert only led to a reduction in subset of lipids (which requires further analysis) and an increase in PtdIns4P on autolysosomes. Therefore, loss of *Sac1* might have additive effects by compromising the activities of both Osbp and cert. Other unknown PtdIns4P effectors might also participate in this process. We cannot exclude the possibility that Osbp and cert can regulate autophagy in both Sac1-dependent and Sac1-independent manners. However, the detailed mechanisms remain unclear.

Although Pi4KII $\alpha$  was the major PtdIns4K required for PtdIns4P accumulation in the autolysosome, Fwd and Pi4KIII $\alpha$

also participated in autophagy in flies. PI4KIII $\beta$  is delivered by ATG9A vesicles to the autophagy initiation site to control PtdIns4P production and recruit the ULK1/2 initiation kinase complex subunit ATG13 to nascent autophagosomes [29]. Our data also suggested that various PtdIns4Ks regulated autophagy differently.

In this study, the distribution of PtdIns4Ks, Osbp, cert, and PtdIns4P was assessed using overexpression proteins or reporters because antibodies recognizing endogenous proteins were lacking. Overexpression of these proteins might cause artifacts that affect the interpretation of the results. Further experiments on the endogenous protein distribution are required to determine the functions of these proteins during autophagy.

In summary, cells reused a set of molecules mediating lipid transfer at the ER-Golgi contacts at the ER-autolysosome contacts by relocating PtdIns4P during autophagy. During revision of this manuscript, Tan et al reported that lysosomal membrane permeabilization stimulates PI4K2A accumulation on damaged lysosomes [42]. PtdIns4P generated by PI4K2A recruits multiple OSBP-related protein family members to establish extensive new membrane contact sites between damaged lysosomes and the ER. Interestingly, cells use an almost identical strategy to establish organelle contacts under different stresses, such as during starvation and lysosomal damage. This strategy is economical and reflects the “small toolkits” principle of evolution.

## Materials and Methods

### Fly strains

Fly strains were maintained on standard *Drosophila* medium at 25°C. The fly strains used in this study were listed in the Table S1. All RNAi stocks were obtained from Tsinghua Fly center. The FLP/FLP recombination target (FRT) stocks and the stocks carrying UAS-autophagy related markers were



obtained from the Bloomington Drosophila Stock Center or generated before in the laboratory. All the transgenic strains were generated by the standard methods, which were constructed by PhiC31-mediated transgenesis to integrate the DNA fragments at specific sites in the genome. Therefore, transgenes presumably were single copy insertions. All transgene vectors constructed in this study were based on the pUAS-attB, p-attB or pCFD5\_w plasmids. The genotypes of fly strains generated in this paper were shown in Table S2–S4.

### Molecular cloning

The plasmid pUAS-attB-HA-Sac1 was generated by cloning *Sac1* cDNA into pUAS-attB vector (from Dr. Hugo Bellen's laboratory, Baylor College of Medicine, USA) with a N-terminal 3×HA tag. The plasmid pUAS-attB-HA-fwd was generated by cloning *fwd* cDNA into pUAS-attB vector with a N-terminal 3×HA tag. The plasmid pUAS-attB-HA-Pi4KIIα was generated by cloning *Pi4KIIα* cDNA into pUAS-attB vector with a N-terminal 3×HA tag. The plasmid pUAS-attB-HA-Pi4KIIIα was generated by cloning *Pi4KIIIα* cDNA into pUAS-attB vector with a N-terminal 3×HA tag. The plasmid pUAS-attB-cert-V5 was generated by cloning *cert* cDNA into pUAS-attB vector with a C-terminal V5 tag. The plasmid pUAS-attB-Osbp-V5 was generated by cloning *Osbp* cDNA into pUAS-attB vector with a C-terminal V5 tag. The plasmids pUAS-attB-Osbp<sup>R34L</sup>-V5 and pUAS-attB-Osbp<sup>CBmu (H503A H504A K713A)</sup>-V5 were generated by site-directed mutagenesis. The plasmid of pUAS-attB-GFP-RFP-Atg8a was generated by cloning the GFP-RFP tandem tag fused to the N-terminus of the coding sequence of Atg8a into pUAS-attB vector. The plasmid p-attB-V5-Sac1 was generated by cloning the genomic sequence of *Sac1* into p-attB vector (from Dr. Hugo Bellen's laboratory), V5 tag was fused to the N terminus of *Sac1*. The plasmid pUAS-attB-Arfip-V5 was generated by cloning *Arfip* cDNA into pUAS-attB vector with a C-terminal V5 tag. The plasmid pCFD5\_w-Osbp sgRNA was generated by cloning the sgRNA of *Osbp* (GAGCTACTACCGCAACCAGT) into pCFD5\_w vector [43]. The plasmid pUAS-attB-GFP-P4M-SidM was generated by cloning GFP-P4M-SidM sequence into pUAS-attB vector.

### Starvation treatment

Embryos were collected within a 6-h period after egg laying and raised on standard fly food at 25°C. After 88–90 h development, third-instar larvae were either fed with normal food or starved in 5 mL 20% sucrose solution to induce autophagy. Fed and starved larvae were then collected for further analysis.

### Immunofluorescence

The third-instar larval fat bodies were dissected in 4% PFA (Sigma-Aldrich, 158127) and incubated for 30 min at room temperature (RT). Then, fat bodies were permeabilized 10 min with PBST (PBS with 0.1% Triton X-100 [Sangon Biotech, T0694]) three times and incubated with primary antibodies with proper dilutions for 2 h at RT, followed by extensive washing. Tissues were incubated with the secondary

antibodies for 1 h at RT in dark. Finally, tissues were washed with PBST three times, mounted in 80% glycerol (Sangon Biotech, A100854) containing 5 ng/μL DAPI (Invitrogen, D-1306) and imaged using LSM710 confocal microscopy (Carl Zeiss, Oberkochen, Germany) with a Plan-Apochromat ×40 or ×63 oil immersion.

### Filipin staining

The third-instar larval fat bodies were dissected in 4% PFA and incubated for 30 min at RT. Tissues were washed three times with PBS and incubated with 50 ng/mL filipin solution for 2 h in a dark chamber. Then, tissues were rinsed three times with PBS and imaged through LSM710 confocal microscopy using a UV filter set (excitation at 340–380 nm and emission at 385–470 nm).

### Determination of lysosomal pH

LysoSensor Yellow/Blue DND-160 (Yeasen, LX4232) was used to measure lysosomal pH. The third-instar larval fat bodies were dissected in PBS and incubated in 1 μM LysoSensor Yellow/Blue DND-160 for 10 min at RT in dark. After washed 3 times with PBS, tissues were mounted in 80% glycerol and imaged with LSM710 confocal microscopy immediately.

### Antibody and probe

Mouse monoclonal antibodies against V5 (Invitrogen, R96025) was used with a 1:500 dilution for immunofluorescence. V5 Tag recombinant rabbit monoclonal antibody (Invitrogen, MA5-32053) was used with 1:500 dilution for immunofluorescence. Purified anti-HA.11 epitope tag (Biolegend, 901501) was used with 1:800 dilution for immunofluorescence. Anti-Cp1/Cathepsin L/MEP antibody (Abcam, ab58991) was used with 1:500 dilution for immunofluorescence. Recombinant Anti-GM130 antibody (Abcam, ab52649) was used with a 1:200 dilution for immunofluorescence. Mouse anti-HRP (Sigma-Aldrich, SAB5300168) was used with 1:500 dilution for immunofluorescence. Mouse anti-Atg8a antibody was generated by the Institute of Genetics and Developmental Biology, CAS and used with 1:500 and 1:1000 dilutions for immunofluorescence and western blot, respectively. Mouse monoclonal antibody against α-tubulin (Beyotime, AT819) was used with 1:1000 dilution for western blot. HRP-labeled Goat Anti-Mouse IgG (Beyotime, A0216) was used with 1:5000 dilution for western blot. Filipin III (APEX-BIO, B6034) was used with 50 ng/mL concentration for fluorescence staining. Ceramide monoclonal antibody (MID 15B4) (Enzo Life, ALX-804-196-T050) was used with 1:10 dilution for immunofluorescence staining. For the secondary antibodies, Alexa Flour 488-conjugated anti-mouse and anti-rabbit IgG (Invitrogen, A-21202 and A-21206), Alexa Flour 647-conjugated anti-mouse and anti-rabbit IgG (Invitrogen, A-21235 and A-31573) and Cy3 AffiniPure Donkey Anti-Mouse IgG (Jackson, 715-165-151): a 1:1000 dilution was used.

### Transmission electron microscopy

For fly eye samples (2 or 31 days), fly heads were dissected and incubated in EM eye solution (containing 1.4% cacodylic acid [Electron Microscopy Sciences, 12201], 4% paraformaldehyde [Electron Microscopy Sciences, 15711], and 1% glutaraldehyde [Electron Microscopy Sciences, 16020]) for 1 week at 4°C. Samples were then washed three times with ddH<sub>2</sub>O, and incubated in 2% OsO<sub>4</sub> (Electron Microscopy Sciences, 19152) for 2 h at RT. After rinsing three times with ddH<sub>2</sub>O, samples were dehydrated by a graded series of ethanol (50%, 70%, 80%, 90%, 95%, and 100%, respectively) for 20 min/step. Then, samples were incubated in propylene oxide (PO, [Sigma, 82320]) for 30 min with three times. After that, samples were infiltrated by a graded series of Eponate 12 resin (50% and 75% in PO) for 3 h/step at RT, embedded in fresh and pure Eponate 12 resin made up with Embed 812 (Electron Microscopy Sciences, 14900), DDSA (Electron Microscopy Sciences, 13710), NMA (Electron Microscopy Sciences, 19000) and DMP-30 (Electron Microscopy Sciences, 13600) for 12 h at RT and polymerized at 65°C for 72 h.

For third-instar larval fat bodies, samples were incubated in 2.5% glutaraldehyde (Electron Microscopy Sciences, 16020) for 48 h and washed with PBS after fixation. All the other steps were same with fly eyes EM protocol.

After polymerization, samples were cut into 50 nm thin sections and stained with 4% uranyl acetate (Electron Microscopy Sciences, 22400) and 2.5% lead nitrate (Electron Microscopy Sciences, 17800) for electron microscopy analysis (Hitachi Ltd., HT7700, Tokyo, Japan).

### Real-time quantitative polymerase chain reaction

The third-instar larval fat bodies were collected and lysed by TRIzol (Invitrogen, 15596026) for extracting total RNA according to the instruction, and the cDNA was synthesized using 4 µg RNA with M-MLV RT kits (Invitrogen, 28025013). The relative expression of 11 genes (*Sac1*, *fwd*, *Pi4KIIα*, *Pi4KIIIα*, *cert*, *Osbp*, *Vap33*, *Syx17*, *Atg1*, *Atg9* and *Atg12*) were measured by PowerSYBR Green PCR Master Mix Kit (Applied Biosystems, 4368708) with specific primers (Table S5). *αTub84B* was used as the internal control. The baseline adjustment method of the BioRadCFX Manager (Bio-Rad, California, USA) was used to determine the Ct of each reaction. The amplification efficiencies were close to 100%, and all samples were amplified in triplicate. For data analysis,  $2^{-\Delta\Delta Ct}$  method was used to calculate the relative level of samples.

### Western blotting

The third-instar larval fat bodies were dissected and lysed using cell lysis buffer for western blot and IP (Beyotime, P0013). Protein samples were separated by a SDS PAGE and then transferred onto a PVDF membrane, followed by blocking with 5% nonfat milk (Sangon Biotech, A600669) in TBST buffer (50 mM Tris-Cl, 150 mM NaCl, 0.1% Tween 20) for 1 h and incubated with primary antibodies overnight at 4°C. The membranes were then washed three times in TBST and incubated with HRP labeled secondary antibodies (1:5000 in TBST

with 5% nonfat milk) for 1 h at RT. The membranes were then washed three times in TBST buffer, incubated with ECL reagent and then exposed.

### Statistical analysis

Confocal, electron microscopy and western blot images were quantified by ImageJ and Zen 2.3 software and analyzed with GraphPad Prism 5 software. To analyze the size and number of protein puncta, images were imported to ImageJ software, and the cytoplasmic part of each cell was selected through polygon selections and then measured the number of puncta and area of single dot under the same threshold for every independent experiment. For fluorescence intensity analysis, images were imported to Zen 2.3 software, and the membrane, cytoplasm or protein dots of each cell were selected using spline contour for detecting fluorescence levels, respectively. For colocalized area measurement, images were imported to Zen 2.3 software, and the colocalized regions between two proteins was selected with spline contour, and then the area of each colocalized region was measured. For flux reporter analysis, the number of yellow puncta that contain both green and red fluorescence and red puncta was counted by hand, and then the frequency of yellow and red puncta was calculated with GraphPad Prism 5 software, respectively. At least three samples for each group were quantified. The two-tailed unpaired Student t test was used for comparisons between two groups, and the ANOVA analysis was used for comparisons of multiple groups. All results were presented as mean values ± standard error of the mean (SEM). *P* value < 0.05 was considered statistically significant.

### Acknowledgements

We are grateful to THFC, BDSC, DGRC, and core facility in LSI, Zhejiang University for providing fly strains, cDNA clones, and technique supports.

### Disclosure statement

No potential conflict of interest was reported by the authors.

### Funding

Dr. Tong Chao is supported by National Natural Science Foundation of China (92254305, 92157201, 32030027, 91754103), Fundamental research funds for the central universities, and Shenzhen Bay Scholars Program. Dr. Liu Hao is supported by National Natural Science Foundation of China (32100599).

### Data availability statement

All data generated in this study have been included in the main text or supplementary materials.

### ORCID

Chao Tong  <http://orcid.org/0000-0001-6521-5465>



## References

- [1] Prinz WA, Toulmay A, Balla T. The functional universe of membrane contact sites. *Nat Rev Mol Cell Biol.* 2020 Jan;21(1):7–24. PubMed PMID: 31732717. doi:10.1038/s41580-019-0180-9.
- [2] Bohnert M. Tether me, tether me not-dynamic organelle contact sites in metabolic rewiring. *Dev Cell.* 2020 Jul 20;54(2):212–225. PubMed PMID: 32693056. doi:10.1016/j.devcel.2020.06.026.
- [3] Wu Y, Whiteus C, Xu CS, et al. Contacts between the endoplasmic reticulum and other membranes in neurons. *Proc Natl Acad Sci, USA.* 2017 Jun 13;114(24):E4859–E4867. PubMed PMID: 28559323; PubMed Central PMCID: PMC5474793. doi: 10.1073/pnas.1701078114
- [4] Cohen S, Valm AM, Lippincott-Schwartz J. Interacting organelles. *Curr Opin Cell Biol.* 2018 Aug;53:84–91. PubMed PMID: 30006038; PubMed Central PMCID: PMC6241252. doi:10.1016/j.ccb.2018.06.003.
- [5] De Vos KJ, Morotz GM, Stoica R, et al. VAPB interacts with the mitochondrial protein PTPIP51 to regulate calcium homeostasis. *Hum Mol Genet.* 2012 Mar 15;21(6):1299–1311. doi:10.1093/hmg/ddr559. PubMed PMID: 22131369; PubMed Central PMCID: PMC3284118.
- [6] Eisenberg-Bord M, Shai N, Schuldiner M, et al. A tether is a tether is a tether: tethering at membrane contact sites. *Dev Cell.* 2016 Nov 21;39(4):395–409. doi:10.1016/j.devcel.2016.10.022. PubMed PMID: 27875684.
- [7] Murphy SE, Levine TP. VAP, a versatile access point for the endoplasmic reticulum: review and analysis of FFAT-like motifs in the VAPome. *Biochim Biophys Acta.* 2016 Aug;1861(8):952–961. PubMed PMID: 26898182. doi:10.1016/j.bbali.2016.02.009.
- [8] Cabukusta B, Berlin I, van Elsland DM, et al. Human VAPome analysis reveals MOSPD1 and MOSPD3 as membrane contact site proteins interacting with FFAT-Related FFNT motifs. *Cell Rep.* 2020 Dec 8;33(10):108475. doi:10.1016/j.celrep.2020.108475. PubMed PMID: 33296653.
- [9] Zhang Y, Liu X, Bai J, et al. Mitoguardin regulates mitochondrial fusion through MitoPLD and is required for neuronal homeostasis. *Molecular Cell.* 2016 Jan 7;61(1):111–124. doi:10.1016/j.molcel.2015.11.017. PubMed PMID: 26711011.
- [10] Xu L, Wang X, Zhou J, et al. Miga-mediated endoplasmic reticulum-mitochondria contact sites regulate neuronal homeostasis. *Elife.* 2020 Jul 10;9. PubMed PMID: 32648543; PubMed Central PMCID: PMC7556861. doi: 10.7554/eLife.56584
- [11] Alpy F, Rousseau A, Schwab Y, et al. STARD3 or STARD3NL and VAP form a novel molecular tether between late endosomes and the ER. *J Cell Sci.* 2013 Dec 1;126(Pt 23):5500–5512. PubMed PMID: 24105263. doi:10.1242/jcs.139295
- [12] Peretti D, Dahan N, Shimoni E, et al. Coordinated lipid transfer between the endoplasmic reticulum and the Golgi complex requires the VAP proteins and is essential for Golgi-mediated transport? *Mol Biol Cell.* 2008 Sep;19(9):3871–3884. PubMed PMID: 18614794; PubMed Central PMCID: PMC2526681. doi:10.1091/mbc.E08-05-0498.
- [13] Nakatogawa H. Mechanisms governing autophagosome biogenesis. *Nat Rev Mol Cell Biol.* 2020 Aug;21(8):439–458. PubMed PMID: 32372019. doi:10.1038/s41580-020-0241-0.
- [14] Dikic I, Elazar Z. Mechanism and medical implications of mammalian autophagy. *Nat Rev Mol Cell Biol.* 2018 Jun;19(6):349–364. PubMed PMID: 29618831. doi:10.1038/s41580-018-0003-4.
- [15] Feng Y, He D, Yao Z, et al. The machinery of macroautophagy. *Cell Res.* 2014 Jan;24(1):24–41. PubMed PMID: 24366339; PubMed Central PMCID: PMC3879710. doi:10.1038/cr.2013.168.
- [16] Zhao YG, Codogno P, Zhang H. Machinery, regulation and pathophysiological implications of autophagosome maturation. *Nat Rev Mol Cell Biol.* 2021 Nov;22(11):733–750. PubMed PMID: 34302147; PubMed Central PMCID: PMC8300085. doi:10.1038/s41580-021-00392-4.
- [17] Hamasaki M, Furuta N, Matsuda A, et al. Autophagosomes form at ER-mitochondria contact sites. *Nature.* 2013 Mar 21;495(7441):389–393. PubMed PMID: 23455425. doi: 10.1038/nature11910
- [18] Gomez-Suaga P, Paillusson S, Stoica R, et al. The ER-Mitochondria tethering complex VAPB-PTPIP51 regulates autophagy. *Curr Biol.* 2017 Feb 6;27(3):371–385. doi:10.1016/j.cub.2016.12.038. PubMed PMID: 28132811; PubMed Central PMCID: PMC5300905.
- [19] Bosc C, Broin N, Fanjul M, et al. Autophagy regulates fatty acid availability for oxidative phosphorylation through mitochondria-endoplasmic reticulum contact sites. *Nat Commun.* 2020 Aug 13;11(1):4056. PubMed PMID: 32792483; PubMed Central PMCID: PMC7426880. doi: 10.1038/s41467-020-17882-2
- [20] Zhao YG, Chen Y, Miao G, et al. The ER-Localized transmembrane protein EPG-3/VMP1 regulates SERCA activity to control ER-Isolation membrane contacts for autophagosome formation. *Molecular Cell.* 2017 Sep 21;67(6):974–989.e6 PubMed PMID: 28890335. doi: 10.1016/j.molcel.2017.08.005
- [21] Zhao YG, Liu N, Miao G, et al. The ER contact proteins VAPA/B interact with multiple Autophagy proteins to modulate Autophagosome Biogenesis. *Curr Biol.* 2018 Apr 23;28(8):1234–1245.e4. PubMed PMID: 29628370. doi: 10.1016/j.cub.2018.03.002
- [22] Zhang H, Zhou J, Xiao P, et al. PtdIns4P restriction by hydrolase SAC1 decides specific fusion of autophagosomes with lysosomes. *Autophagy.* 2021 Aug;17(8):1907–1917. PubMed PMID: 32693712; PubMed Central PMCID: PMC8386628. doi:10.1080/15548627.2020.1796321.
- [23] Mesmin B, Bigay J, Moser von Filseck J, et al. A four-step cycle driven by PI(4)P hydrolysis directs sterol/PI(4)P exchange by the ER-Golgi tether OSBP. *Cell.* 2013 Nov 7;155(4):830–843. PubMed PMID: 24209621. doi:10.1016/j.cell.2013.09.056
- [24] Balla A, Balla T. Phosphatidylinositol 4-kinases: old enzymes with emerging functions. *Trends in cell biology.* 2006 Jul;16(7):351–361. PubMed PMID: 16793271. doi: 10.1016/j.tcb.2006.05.003
- [25] D'Angelo G, Vicinanza M, Di Campli A, et al. The multiple roles of PtdIns(4)P – not just the precursor of PtdIns(4,5)P2. *J Cell Sci.* 2008 Jun 15;121(Pt 12):1955–1963. PubMed PMID: 18525025. doi: 10.1242/jcs.023630
- [26] Graham TR, Burd CG. Coordination of Golgi functions by phosphatidylinositol 4-kinases. *Trends in cell biology.* 2011 Feb;21(2):113–121. PubMed PMID: 21282087; PubMed Central PMCID: PMC3053015. doi: 10.1016/j.tcb.2010.10.002
- [27] Wang K, Yang Z, Liu X, et al. Phosphatidylinositol 4-kinases are required for autophagic membrane trafficking. *J Biol Chem.* 2012 Nov 2;287(45):37964–37972. PubMed PMID: 22977244; PubMed Central PMCID: PMC3488067. doi:10.1074/jbc.M112.371591
- [28] Wang H, Sun HQ, Zhu X, et al. Gabaraps regulate PI4P-dependent autophagosome: lysosome fusion. *Proc Natl Acad Sci, USA.* 2015 Jun 2;112(22):7015–7020. PubMed PMID: 26038556; PubMed Central PMCID: PMC4460452. doi: 10.1073/pnas.1507263112
- [29] Judith D, Jefferies HBJ, Boeing S, et al. ATG9A shapes the forming autophagosome through Arfaptin 2 and phosphatidylinositol 4-kinase IIIbeta. *J Cell Bio.* 2019 May 6;218(5):1634–1652. PubMed PMID: 30917996; PubMed Central PMCID: PMC6504893. doi: 10.1083/jcb.201901115
- [30] Rahajeng J, Kuna RS, Makowski SL, et al. Efficient Golgi forward trafficking requires GOLPH3-driven, PI4P-Dependent membrane curvature. *Dev Cell.* 2019 Sep 9;50(5):573–585.e5. PubMed PMID: 31231041; PubMed Central PMCID: PMC7583631. doi: 10.1016/j.devcel.2019.05.038
- [31] Ghabrial AS, Levi BP, Krasnow MA, et al. A systematic screen for tube morphogenesis and branching genes in the *Drosophila* tracheal system. *PLoS Genet.* 2011 Jul;7(7):e1002087. PubMed PMID: 21750678; PubMed Central PMCID: PMC3131284. doi:10.1371/journal.pgen.1002087.
- [32] Takats S, Nagy P, Varga A, et al. Autophagosomal Syntaxin17-dependent lysosomal degradation maintains neuronal function in *Drosophila*. *J Cell Bio.* 2013 May 13;201(4):531–539. PubMed PMID: 23671310; PubMed Central PMCID: PMC3653357. doi: 10.1083/jcb.201211160

- [33] Hama H, Schnieders EA, Thorner J, et al. Direct involvement of phosphatidylinositol 4-phosphate in secretion in the yeast *Saccharomyces cerevisiae*. *J Biol Chem*. 1999 Nov 26;274(48):34294–34300. doi:[10.1074/jbc.274.48.34294](https://doi.org/10.1074/jbc.274.48.34294). PubMed PMID: 10567405.
- [34] Hammond GR, Machner MP, Balla T. A novel probe for phosphatidylinositol 4-phosphate reveals multiple pools beyond the Golgi. *J Cell Bio*. 2014 Apr 14;205(1):113–126. PubMed PMID: 24711504; PubMed Central PMCID: PMC3987136. doi: [10.1083/jcb.201312072](https://doi.org/10.1083/jcb.201312072)
- [35] Balakrishnan SS, Basu U, Raghu P. Phosphoinositide signalling in *Drosophila*. *Biochimica et Biophysica Acta (BBA) - Mol Cell Biol Lipids*. 2015 Jun;1851(6):770–784. PubMed PMID: 25449646. doi:[10.1016/j.bbalip.2014.10.010](https://doi.org/10.1016/j.bbalip.2014.10.010).
- [36] Mao D, Lin G, Tepe B, et al. VAMP associated proteins are required for autophagic and lysosomal degradation by promoting a PtdIns4P-mediated endosomal pathway. *Autophagy*. 2019 Jul;15(7):1214–1233. PubMed PMID: 30741620; PubMed Central PMCID: PMC6613884. doi:[10.1080/15548627.2019.1580103](https://doi.org/10.1080/15548627.2019.1580103).
- [37] Zhao K, Ridgway ND. Oxysterol-binding protein-related protein 1L regulates cholesterol egress from the endo-lysosomal system. *Cell Rep*. 2017 May 30;19(9):1807–1818. PubMed PMID: 28564600. doi:[10.1016/j.celrep.2017.05.028](https://doi.org/10.1016/j.celrep.2017.05.028).
- [38] Hoglinger D, Burgoyne T, Sanchez-Heras E, et al. NPC1 regulates ER contacts with endocytic organelles to mediate cholesterol egress. *Nat Commun*. 2019 Sep 19;10(1):4276. PubMed PMID: 31537798; PubMed Central PMCID: PMC6753064. doi: [10.1038/s41467-019-12152-2](https://doi.org/10.1038/s41467-019-12152-2)
- [39] Lim CY, Davis OB, Shin HR, et al. ER-lysosome contacts enable cholesterol sensing by mTORC1 and drive aberrant growth signalling in Niemann-pick type C. *Nat Cell Biol*. 2019 Oct;21(10):1206–1218. PubMed PMID: 31548609; PubMed Central PMCID: PMC6936960. doi:[10.1038/s41556-019-0391-5](https://doi.org/10.1038/s41556-019-0391-5).
- [40] Lu A, Hsieh F, Sharma BR, et al. CRISPR screens for lipid regulators reveal a role for ER-bound SNX13 in lysosomal cholesterol export. *J Cell Bio*. 2022 Feb 7;221(2). PubMed PMID: 34936700; PubMed Central PMCID: PMC8704955. doi: [10.1083/jcb.202105060](https://doi.org/10.1083/jcb.202105060)
- [41] Liu K, Kong L, Graham DB, et al. SAC1 regulates autophagosomal phosphatidylinositol-4-phosphate for xenophagy-directed bacterial clearance. *Cell Rep*. 2021 Jul 27;36(4):109434. PubMed PMID: 34320354; PubMed Central PMCID: PMCPCMC8327279. doi:[10.1016/j.celrep.2021.109434](https://doi.org/10.1016/j.celrep.2021.109434).
- [42] Tan JX, Finkel T. A phosphoinositide signalling pathway mediates rapid lysosomal repair. *Nature*. 2022 Sep;609(7928):815–821. PubMed PMID: 36071159; PubMed Central PMCID: PMCPCMC9450835 Generian Pharmaceuticals. doi:[10.1038/s41586-022-05164-4](https://doi.org/10.1038/s41586-022-05164-4).
- [43] Port F, Bullock SL. Augmenting CRISPR applications in *Drosophila* with Trna-flanked sgRNAs. *Nat Methods*. 2016 Oct;13(10):852–854. PubMed PMID: 27595403; PubMed Central PMCID: PMC5215823. doi:[10.1038/nmeth.3972](https://doi.org/10.1038/nmeth.3972).